

3 Experimental Tools in Nanophotonics I: Far-field Techniques

Highlights of this chapter: In this chapter an important far-field technique, confocal microscopy, is introduced. The technique can be applied to detect single molecules and to trap small particles. We also discuss advanced far-field methods with enhanced optical resolution.

3.1 Confocal microscopy

3.1.1 Point-spread-function of a dipole

We first consider the point-spread-function (PSF) of a single dipole emitter $\boldsymbol{\mu}$. Imaging may occur via a typical microscope lens:

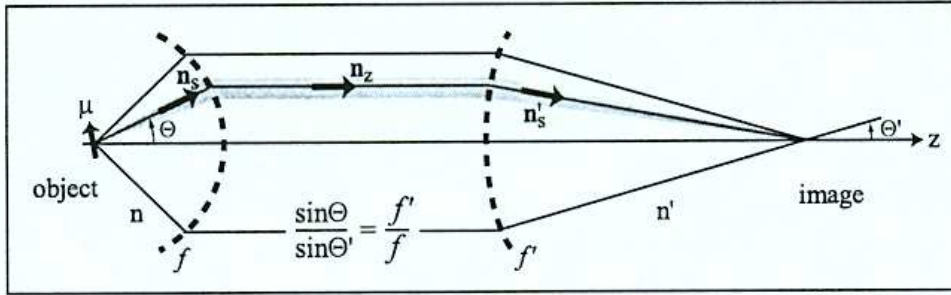


Figure 28: Imaging of a dipole emitter with two lenses of focal length f and f' , respectively. From [Novotny and Hecht, "Principles of Nano-Optics"]

For a dipole $\boldsymbol{\mu}$ of arbitrary orientation at the location r_0 we can write the electric field at r as follows:

$$E(r) = \omega^2 \mu_0 \overleftrightarrow{G}(r, r_0) \boldsymbol{\mu} \quad (167)$$

Here, \overleftrightarrow{G} represents a dyadic Green's tensor. In polar coordinates (and with $r_0 = 0$) at large distance between dipole and lens (compared to the optical wavelength) the tensor has the following form (see also Novotny and Hecht, "Principles of Nano-

Optics”):

$$\begin{aligned} \overleftrightarrow{G}(r, 0) = & \quad (168) \\ \frac{\exp(ikr)}{4\pi r} & \begin{pmatrix} (1 - \cos^2 \phi \sin^2 \vartheta) & -\sin \phi \cos \phi \sin^2 \vartheta & -\cos \phi \sin \vartheta \cos \vartheta \\ -\sin \phi \cos \phi \sin^2 \vartheta & (1 - \sin^2 \phi \sin^2 \vartheta) & -\sin \phi \sin \vartheta \cos \vartheta \\ -\cos \phi \sin \vartheta \cos \vartheta & -\sin \phi \sin \vartheta \cos \vartheta & \sin^2 \vartheta \end{pmatrix} \end{aligned}$$

Similar to the theoretical description of focussed Gaussian beams it is straightforward to write down the field right after the first lens. In case of a dipole oriented parallel to the x -axis ($\mu = \mu_x \hat{n}_x$) we find:

$$\begin{aligned} E_\infty^{(x)}(\vartheta, \phi) = & \quad (169) \\ -\omega^2 \mu_0 \mu_x \frac{\exp(ikf)}{8\pi f} & \begin{pmatrix} (1 + \cos \vartheta \cos \vartheta') - (1 - \cos \vartheta \cos \vartheta') \cos 2\phi \\ -(1 - \cos \vartheta \cos \vartheta') \sin 2\phi \\ 2 \cos \vartheta \sin \vartheta' \cos \phi \end{pmatrix} \sqrt{\frac{n \cos \vartheta'}{n' \cos \vartheta}} \end{aligned}$$

where

$$\sin \vartheta' = \frac{f}{f'} \sin \vartheta \quad (170)$$

$$\cos \vartheta' = \sqrt{1 - (f/f')^2 \sin^2 \vartheta} \quad (171)$$

For a dipole with arbitrary orientation ($\mu = (\mu_x, \mu_y, \mu_z)$) it follows:

$$E_\infty(\vartheta, \phi) = E_\infty^{(x)}(\vartheta, \phi) + E_\infty^{(y)}(\vartheta, \phi) + E_\infty^{(z)}(\vartheta, \phi) \quad (172)$$

This expression can be inserted in the expression for the electric field $E(r)$ expressed via the far-field $E_\infty(\vartheta, \phi)$ as derived in Chapter 2. In the limit $f' \gg f$ one finds:

$$E(\rho, \phi, \vartheta) = \omega^2 \mu_0 \overleftrightarrow{G}_{PSF}(\rho, \phi, \vartheta) \boldsymbol{\mu} \quad (173)$$

with the *dyadic point spread function*

$$\begin{aligned} \overleftrightarrow{G}_{PSF}(\rho, \phi, \vartheta) = & \quad (174) \\ \frac{k'}{8\pi i} \frac{f}{f'} e^{i(kf - k'f')} & \begin{pmatrix} (I_{00} + I_{02} \cos 2\phi) & I_{02} \sin 2\phi & -2iI_{01} \cos \phi \\ I_{02} \sin 2\phi & (I_{00} - I_{02} \cos 2\phi) & -2iI_{01} \sin \phi \\ 0 & 0 & 0 \end{pmatrix} \sqrt{\frac{n}{n'}} \end{aligned}$$

Here we used the integrals:

$$I_{00} = \int_0^{\vartheta_{\max}} (\cos \theta)^{1/2} \sin \theta (1 + \cos \theta) J_0(k' \rho \sin \vartheta f/f') \times \exp(i k' z [1 - 1/2(f/f')^2 \sin^2 \vartheta]) d\vartheta \quad (175)$$

$$I_{01} = \int_0^{\vartheta_{\max}} (\cos \theta)^{1/2} \sin^2 \theta J_1(k' \rho \sin \vartheta f/f') \times \exp(i k' z [1 - 1/2(f/f')^2 \sin^2 \vartheta]) d\vartheta \quad (176)$$

$$I_{02} = \int_0^{\vartheta_{\max}} (\cos \theta)^{1/2} \sin \theta (1 - \cos \vartheta) J_2(k' \rho \sin \vartheta f/f') \times \exp(i k' z [1 - 1/2(f/f')^2 \sin^2 \vartheta]) d\vartheta \quad (177)$$

Remark: The z -component in the far-field is zero as expected.

The PSF depends on the **numerical aperture**

$$NA = n \sin \vartheta_{\max} \quad (178)$$

and the (transversal) **magnification** of the optical system

$$M = \frac{n f'}{n' f} \quad (179)$$

In paraxial approximation ($\sin \vartheta \simeq \vartheta$, $\cos \vartheta = 1$) one finds for a **dipole oriented perpendicular to the x -axis** the transversal field as:

$$\lim_{\vartheta_{\max} \ll \pi/2} |E(x, y, z = 0)|^2 = \frac{\pi^4}{\varepsilon_0^2 n n'} \frac{\mu_x^2}{\lambda^6} \frac{NA^4}{M^2} \left[2 \frac{J_1(2\pi\tilde{\rho})}{(2\pi\tilde{\rho})} \right]^2; \quad \tilde{\rho} = \frac{NA}{M} \frac{\rho}{\lambda} \quad (180)$$

And the longitudinal field as:

$$\lim_{\vartheta_{\max} \ll \pi/2} |E(x = 0, y = 0, z)|^2 = \frac{\pi^4}{\varepsilon_0^2 n n'} \frac{\mu_x^2}{\lambda^6} \frac{NA^4}{M^2} \left[\frac{\sin(\pi\tilde{z})}{(\pi\tilde{z})} \right]^2; \quad \tilde{z} = \frac{NA^2}{2n'M^2} \frac{z}{\lambda} \quad (181)$$

For a **dipole oriented parallel to the z -axis** the transversal field is:

$$\lim_{\vartheta_{\max} \ll \pi/2} |E(x, y, z = 0)|^2 = \frac{\pi^4}{\varepsilon_0^2 n^3 n'} \frac{\mu_z^2}{\lambda^6} \frac{NA^6}{M^2} \left[2 \frac{J_2(2\pi\tilde{\rho})}{(2\pi\tilde{\rho})} \right]^2; \quad \tilde{\rho} = \frac{NA}{M} \frac{\rho}{\lambda} \quad (182)$$

the following figure 29 plots the field for these three cases:

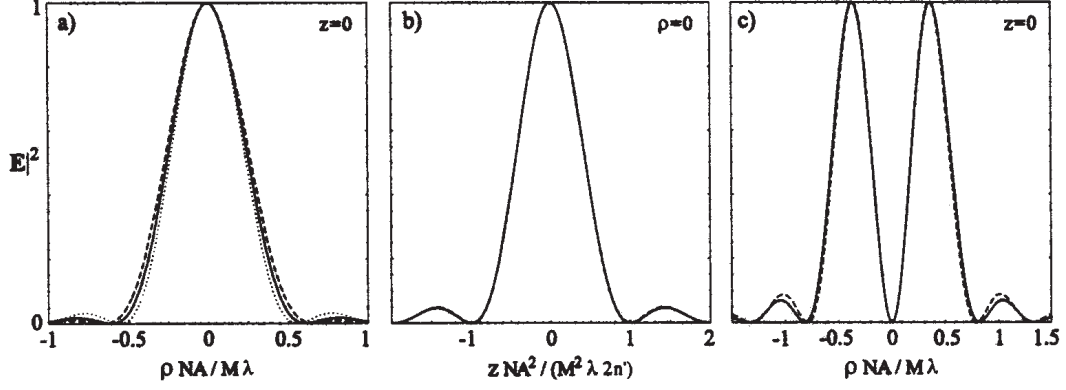


Figure 29: PSF for a dipole perpendicular to the optical axis in the image plane (a) and along the optical axis (b). Dashed and dotted, respectively, is the exact solution parallel and perpendicular to the direction of polarization. The solid line is the paraxial approximation. c) plots the field of a dipole oriented parallel to the optical axis ($NA=1.4$, $n=1.5$).

The ellipticity of the focal spot increases with increasing NA. However, even with a quite large NA the paraxial approximation is acceptable.

For a dipole oriented perpendicular to the optical axis (x - or y -dipole) the distance to the first zero in the diffraction image is:

$$\Delta x = 0.61 \frac{M\lambda}{NA} \quad (183)$$

and

$$\Delta z = 2n' \frac{M^2\lambda}{NA^2} \quad (184)$$

, respectively.

The quantity Δz is denoted as **depth of focus**. Typically, Δz is much larger than Δx .

Example: For a typical microscope objective with $M = 60\times$ and $NA = 1.4$ at $500nm$ it is $\Delta x \approx 13\mu m$, but $\Delta z \approx 1.8mm$

3.1.2 Principle of confocal microscopy

The following figure 30 shows a schematic of a microscope.

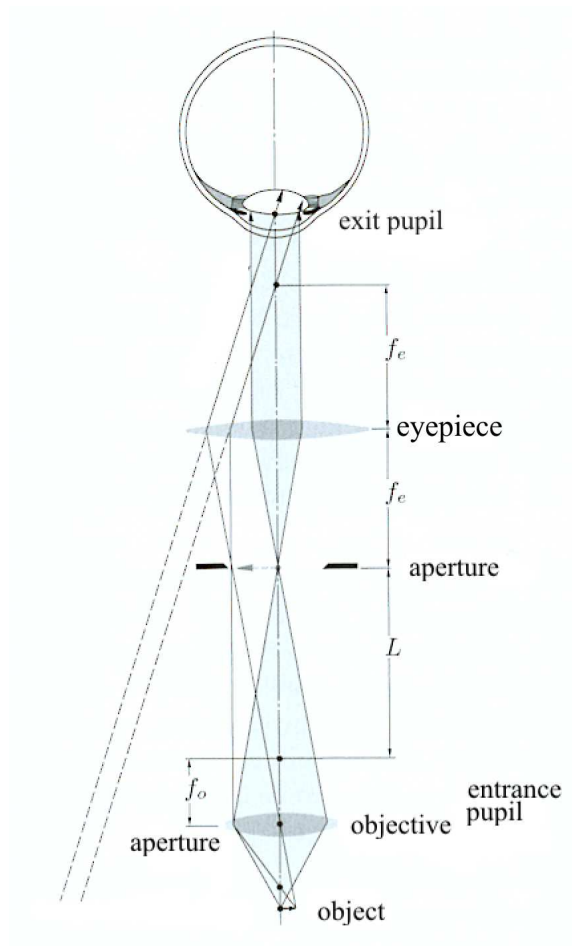


Figure 30: Schematic of a microscope [from Hecht "Optik"].

The objective produces an intermediate image of the object in the plane of the aperture. The intermediate image is magnified by the eyepiece.

The total magnification of the microscope is the product of the magnification of the objective and the eyepiece:

$$M = \left(-\frac{L}{f_o}\right) \left(\frac{254mm}{f_e}\right) \quad (185)$$

Here the standard distance (when viewing a near object) is set to 254 mm. The distance L between the focal points is mostly standardized to 160 mm. An objective with a focal length of, e.g., $f_0 = 32 \text{ mm}$ thus has the classification $5\times$. With an eyepiece with $f_e = 2,54 \text{ cm}$ the resulting magnification is 50. The resolution limit of an optical system, such as a microscope, has been discussed in previous chapters.

In contrast to a conventional microscope, which provides a complete image, the **confocal microscope** images point-wise. Therefore, a scanning of the image is required. The principle steps to realize confocal microscopy is illustrated in figure 31.

- A lens images two points within a thick sample.
- A **pinhole** in the conjugated plane blocks light of all points which are not within the focus.
- If in addition the excitation is **confocal**, then the signal from points not within the focal volume is further suppressed.
- A beam splitter allows excitation and detection via a single lens.

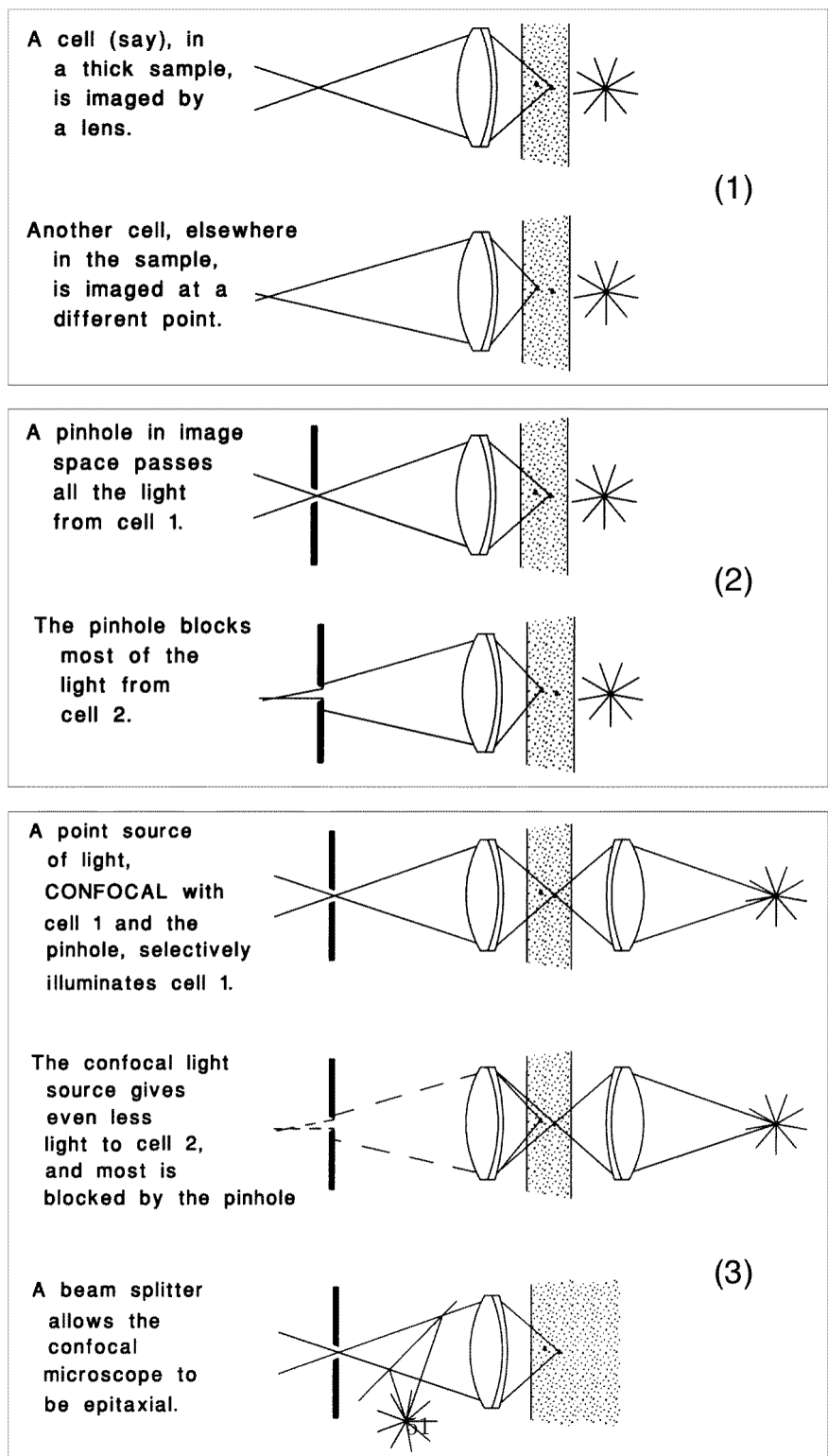


Figure 31: Principle of confocal microscopy [R. H. Webb, Rep. Prog. Phys. 1996].

The following figure 32 illustrates a typical confocal configuration:

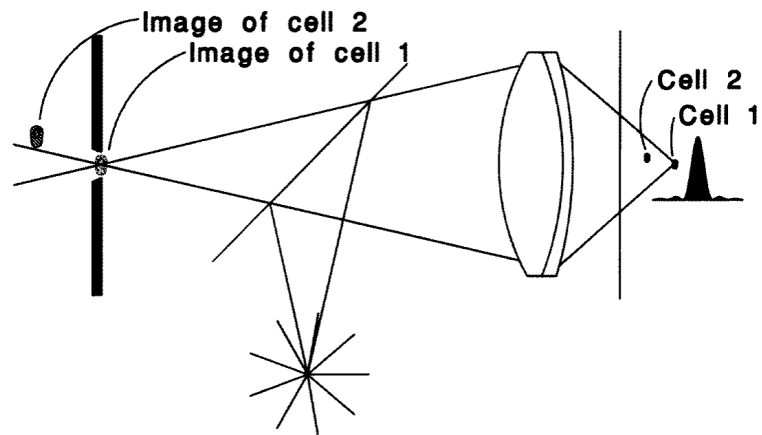


Figure 32: Principle of a confocal microscope [R. H. Webb, Rep. Prog. Phys. 1996].

An essential point in confocal microscopy is that there is no contribution from object points outside of the focal volume. This contrasts usual microscopy.

3.1.3 Resolution in confocal microscopy

The point-spread-function (PSF) of a confocal microscope is the product of the PSF_{point} of imaging the object point and the PSF_{source} of the point-like illumination source (imaged on the object point):

$$PSF(\zeta, \rho)_{conf} = PSF_{point}(\zeta, \rho) \times PSF_{source}(\zeta, \rho) = PSF_{point}^2(\zeta, \rho) \quad (186)$$

We use conveniently scaled units:

$$\zeta = \frac{2\pi}{n\lambda} NA^2 z \quad (187)$$

$$\rho = \frac{2\pi}{\lambda} NA r \quad (188)$$

$$NA = n \sin \vartheta \quad (189)$$

It is

$$PSF_{point}(0, \rho) = 2J_1^2(\rho)/\rho^2 \quad (190)$$

$$PSF_{point}(\zeta, 0) = \left(\sin \frac{\zeta}{4} / \frac{\zeta}{4} \right)^2 \quad (191)$$

The square of PSF leads to an enhanced optical resolution as depicted in figure 33:

$$\Delta r = 0.61 \frac{\lambda}{NA} \quad (192)$$

$$\Delta r_{conf} = 0.44 \frac{\lambda}{NA} \quad (193)$$

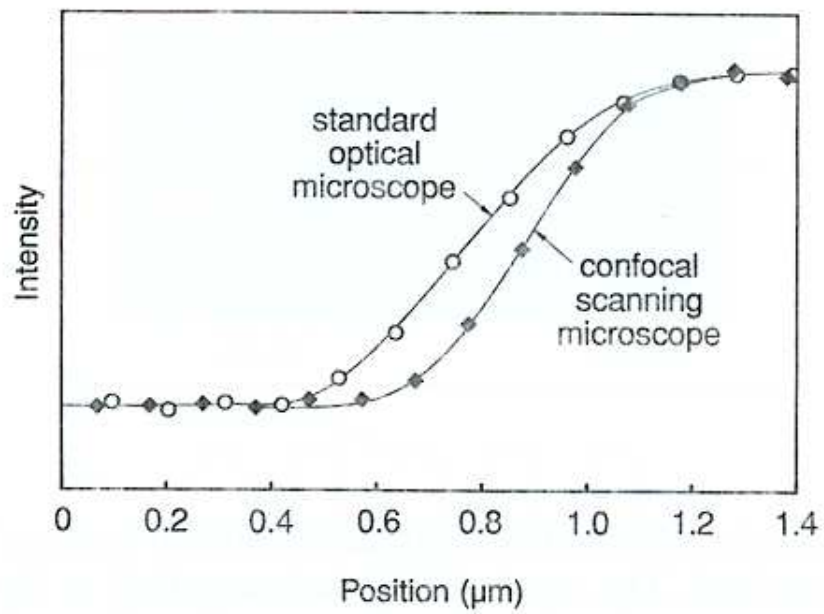


Figure 33: Improved resolution in a confocal microscope [from Corle and Kino "Confocal Scanning Optical Microscopy"].

Figures 34, 35 and 36 show the PSF and its square in the focal plane and along the optical axis:

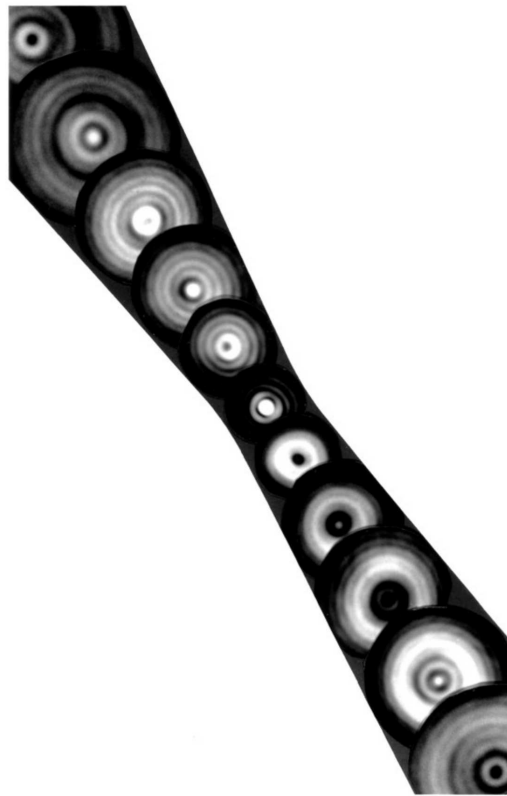


Figure 34: PSF in the proximity of the focus for different ζ along the optical axis [R. H. Webb, Rep. Prog. Phys. 1996].

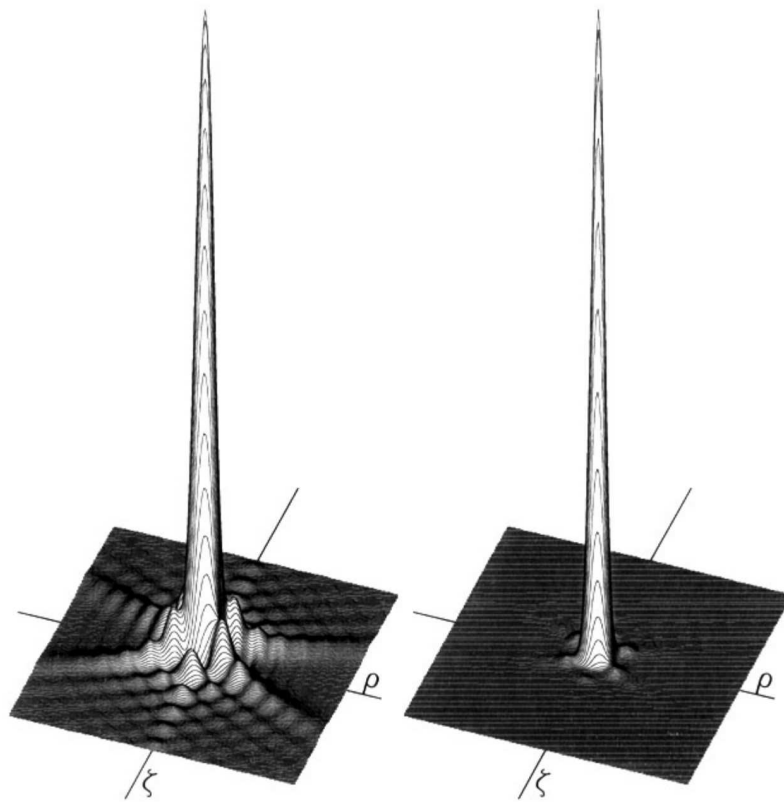


Figure 35: PSF (left) and PSF^2 (right) [R. H. Webb, Rep. Prog. Phys. 1996].

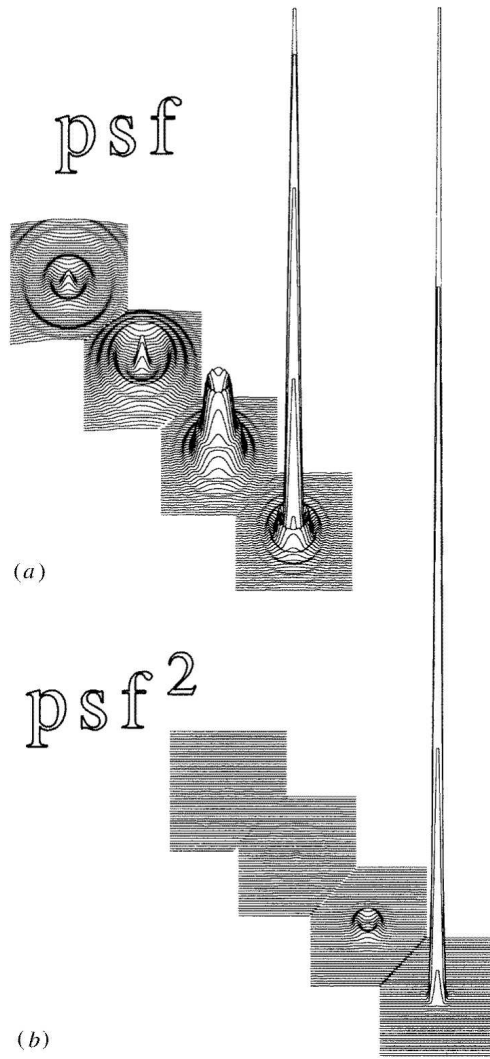


Figure 36: PSF and PSF^2 in the proximity of the focus for different ζ along the optical axis [R. H. Webb, Rep. Prog. Phys. 1996].

A more relevant effect than the enhanced resolution is the suppression of side-maxima, which allows the detection of weak objects even in close proximity to bright objects.

In ordinary microscopy the intensity integrated over a transversal plane is constant:

$$\int_0^{\infty} PSF_{point}(\zeta, \rho) \rho d\rho = const. \quad \text{for all } \zeta \quad (194)$$

This is a consequence of conservation of the energy flux. It is not the case in confocal microscopy as the pinhole selects out only a finite volume.

In a confocal microscope there is a true axial resolution:

$$\Delta z_{conf} = 1.5 \frac{n\lambda}{NA^2} \quad (195)$$

We highlight this aspect of confocal microscopy for imaging a dipole:

Equation 173 gives the electric field of an arbitrary dipole. If there is no pinhole, then an integration over a transversal plane results in a total intensity ($S(z)$):

$$\begin{aligned} S(z) &= \int_0^{2\pi} \int_0^{\infty} E(\rho, \phi, z) E^*(\rho, \phi, z) \rho d\rho d\phi dz = \\ &= \frac{\pi^4}{24\varepsilon_0^2 \lambda^4} [(\mu_x^2 + \mu_y^2)(28 - 12 \cos \vartheta_{\max} - 12 \cos^2 \vartheta_{\max} - 4 \cos^3 \vartheta_{\max}) \\ &\quad + \mu_z^2(8 - 9 \cos \vartheta_{\max} + \cos 3\vartheta_{\max})] \end{aligned} \quad (196)$$

The signal does not contain any information on the z -direction!

However, if we introduce a pinhole which approximately detects only the field on the optical axis, we find:

$$dS(z) = E(\rho = 0, z) E^*(\rho = 0, z) dA = \quad (197)$$

$$\frac{\pi^4}{\varepsilon_0^2 n^2} \frac{\mu_x^2 + \mu_y^2}{\lambda^6} NA^4 \left[\frac{\sin \zeta/4}{\zeta/4} \right]^2 \quad (198)$$

Obviously, there is a clear z -dependence and thus an axial resolution Δz .

In order to calculate imaging by a confocal microscope three steps are required::

1. Calculation of the exciting field in the object plane, i.e., the excitation PSF_{source} . The intensity in the object plane is a convolution:

$$S_{objekt}(\rho, \zeta) = \int S_{source}(\rho_s, \phi_s) PSF_{source}(\rho - \rho_s, \zeta) \rho_s d\phi_s d\rho_s \quad (199)$$

2. Calculation of the *interaction* with the illuminated object ($O(\rho, \zeta)$): This can be a simple point-like interaction (e.g. an excitation followed by fluorescence):

$$\tilde{O}(\rho, \phi, \zeta) = O(\rho, \phi, \zeta) S_{objekt}(\rho, \zeta) \quad (200)$$

3. Calculation of the imaging to the image plane, i.e., PSF_{point} under the condition of the selectivity of the pinhole ($D(\rho, Z)$): This can also be described via a convolution

$$S_{image}(\rho', \phi', \zeta - Z) = \int \tilde{O}(\rho, \phi, \zeta) PSF_{point}(\rho' - \rho, \phi' - \phi, \zeta - Z) \rho d\phi d\rho d\zeta \quad (201)$$

followed by an integration over the pinhole function and all object planes:

$$S_{det}(Z) = \int S_{image}(\rho', \phi', \zeta - Z) D(\rho', \phi') \rho' d\phi' d\rho' d\zeta \quad (202)$$

Remark: A similar situation as in confocal excitation occurs if the interaction between object an excitation light is non-linear (e.g. in two-photon absorption). Also in this case the square of PSF has to be regarded!

3.1.4 Experimental realization and applications

Figure 37 introduces the required components of a Scanning Confocal Optical Microscope, SCOM:

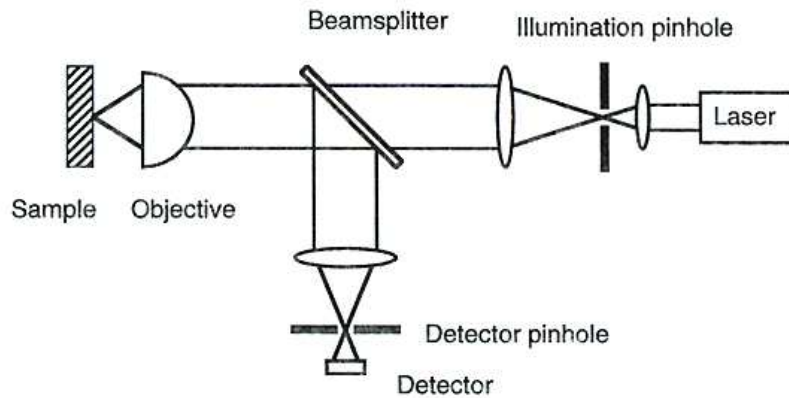


Figure 37: Schematic of a scanning confocal microscope [from Corle and Kino "Confocal Scanning Optical Microscopy"].

The first component is a point-like **illumination source**. A focussed laser beam or an optical fiber is appropriate. When focussing a Gaussian beam the illumination of the collimating lens is an important parameter: An over-illumination results in a diffraction limited spot, an under-illumination results in a maximum power transfer and a Gaussian PSF (without additional side-maxima as in an Airy pattern).

The following figure 38 shows the PSF for different numerical apertures and different filling factors:

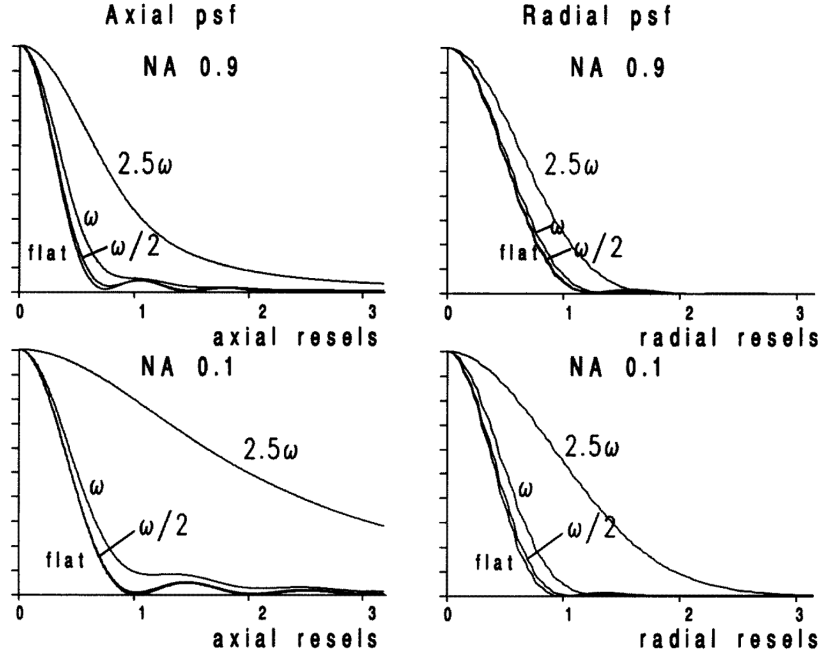


Figure 38: PSF_{source} for different filling factors $\omega = 1$ the radius if the entrance pupil is equal to the $1/e^2$ value of the Gaussian beam profile. Upper row: $NA = 0.9$. Lower row: $NA = 0.1$ [R. H. Webb, Rep. Prog. Phys. 1996].

A main component of a SCOM is the **pinhole**. Both for the excitation and for the detection a pinhole can be used. The detection pinhole should have the size of the Airy disc. A further reduction does not increase the resolution, but decreases the signal. As a larger pinhole increases the signal, there is some trade-off between signal strength and resolution.

The PSF has to be modified if the pinhole is larger than the Airy disc:

$$PSF(\zeta, \rho)_{conf} = PSF_{fold}(\zeta, \rho) \times PSF_{source}(\zeta, \rho) \neq PSF_{point}^2(\zeta, \rho) \quad (203)$$

$PSF_{fold}(\zeta, \rho)$ is calculated as a convolution of the area of the pinhole and the Airy

disc and describes the size of the detectable volume. The following figure 39 shows an example for a pinhole 5-times the size of the Airy disc.

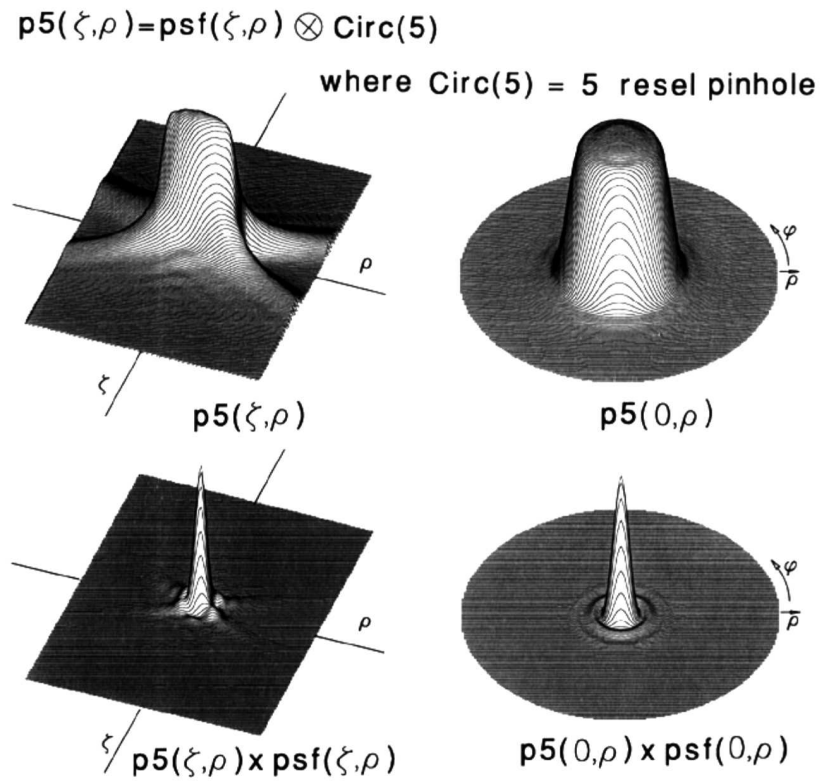


Figure 39: Upper row: Convolution of $\text{PSF}_{\text{point}}$ with the area of the pinhole. Lower row: Resulting PSF_{conf} . [R. H. Webb, Rep. Prog. Phys. 1996].

In contrast to an ordinary microscope a SCOM provides an image point-by-point. A scanning of the probe is required. There are three possibilities for scanning:

1. The probe is scanned (**stage scanning**):

The following figure 40 shows a schematic of a piezo-electric scanning stage:

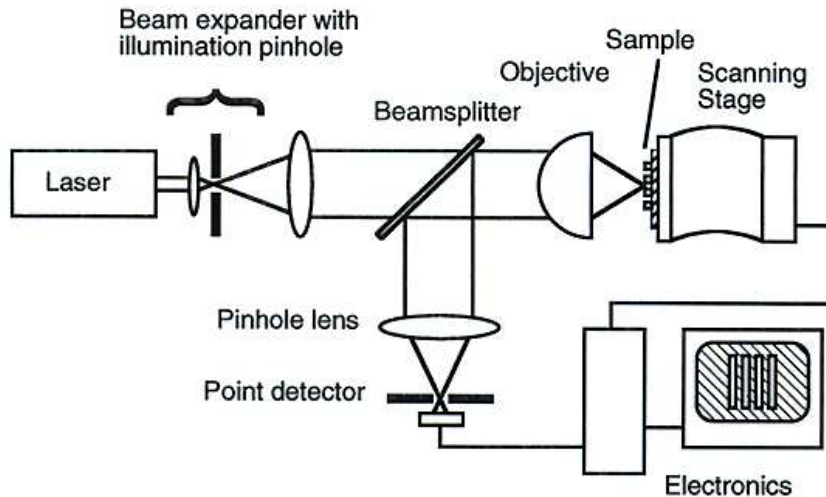


Figure 40: Stage scanning confocal microscope [from Corle and Kino "Confocal Scanning Optical Microscopy"]

A disadvantage of stage scanning is the small scanning speed. If a scanning of 500×500 pixels separated by $1 \mu m$ in 1 sec is desired, then the probe is subjected to an acceleration of $500 g$!

2. Scanning via beam deflection (**beam scanning**):

In this case scanning with a video rate is possible. Beam deflection can be obtained via galvo drives (as in a laser show) or via a scanning lens.

If two galvo mirrors are used for deflection in x - and y -direction, respectively, a telecentric system images the turning point (on the scanner mirror) to the back focal plane of the microscope. The magnification of the objective, the dimension of the mirrors and other optical elements have to be matched to avoid cut-offs and diffraction of the beam. An increase or decrease of the beam diameter can be obtained via telescope lenses. Figure 41 show a possible setup:

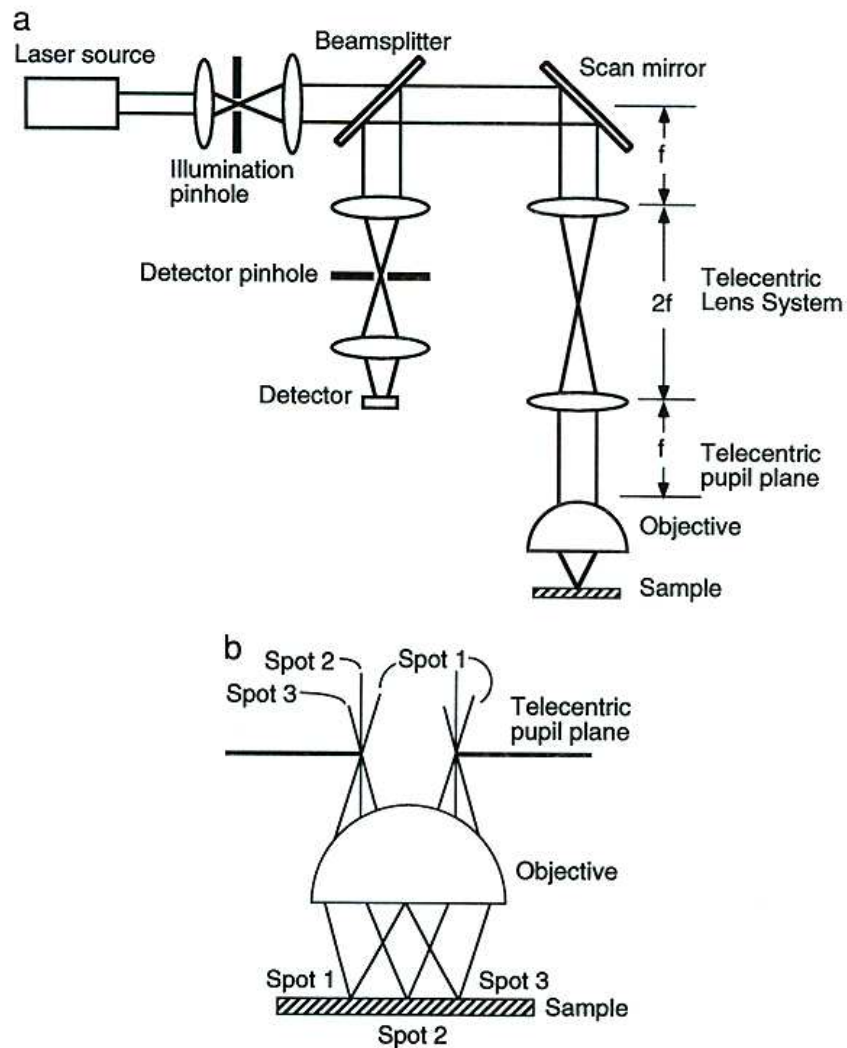


Figure 41: Beam scanning confocal microscope [from Corle and Kino "Confocal Scanning Optical Microscopy"]

3. Scanning of the pinhole (**pinhole scanning**):

In this case the pinholes on the excitation and detection side are scanned synchronously (condition of confocal microscope!). In the configuration shown in figure 42 suggested by Kino a common pinhole is used for both excitation and detection. A complicated alignment is obsolete. If the scanning speed is fast

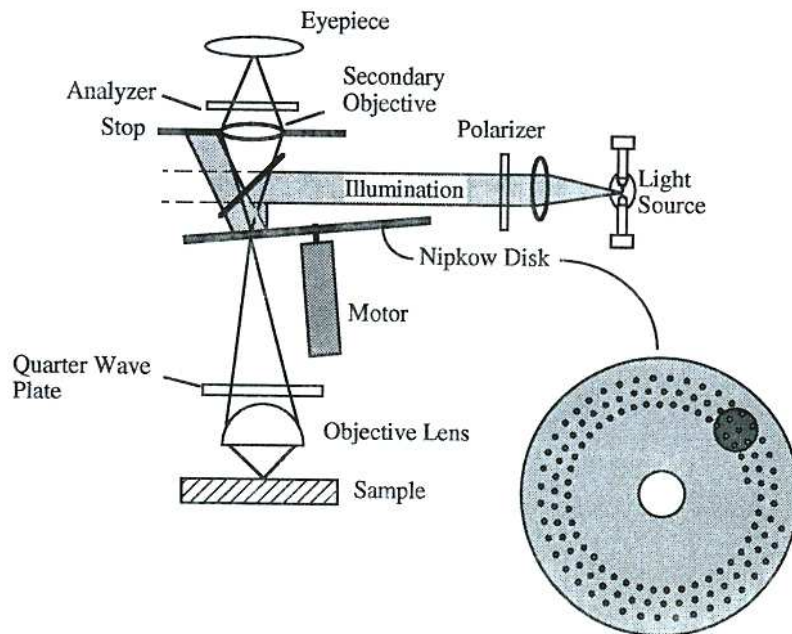


Figure 42: Pinhole scanning confocal microscope [from Corle and Kino "Confocal Scanning Optical Microscopy"]

enough (e.g. when using a Nipkow-disc with small holes in spirals) a direct observation with the bare eye is possible. The eye does not detect the rotation of the disc and there is the perception of a high contrast image.

An additional component of a SCOM is the **detector**. Because of the weak signals photomultiplier or avalanche photodiodes (APDs) with high efficiency are used.

In confocal **fluorescence microscopy** a **dichroic mirror** is often used together with additional spectral filters to separate the excitation light from the fluorescence signal.

In the following we provide several examples for applications of confocal microscopy:

Metrology of solid-state structures:

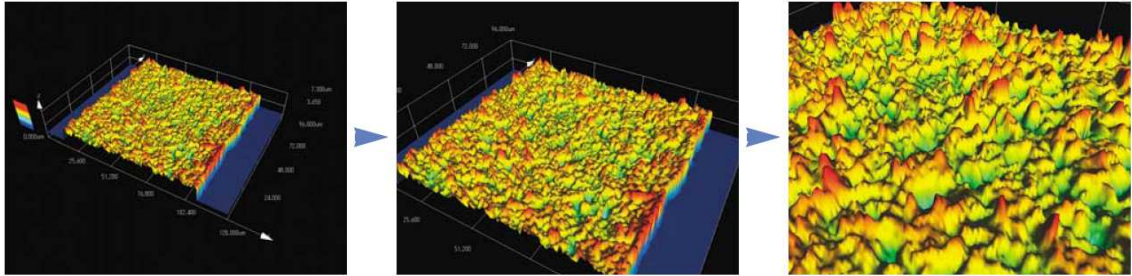
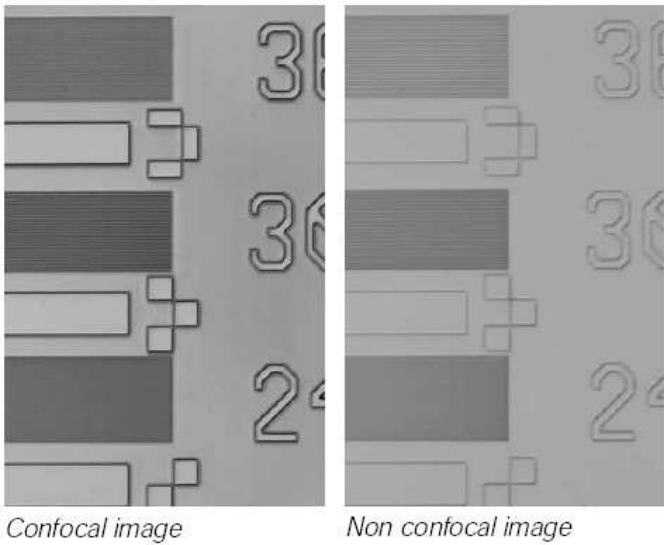


Figure 43: Upper image: Circuit papers on a wafer on a wafer. Bottom image: Surface quality of an electrode. [from Olympus, LEXT brochure]

Three-dimensional imaging of biological probes:

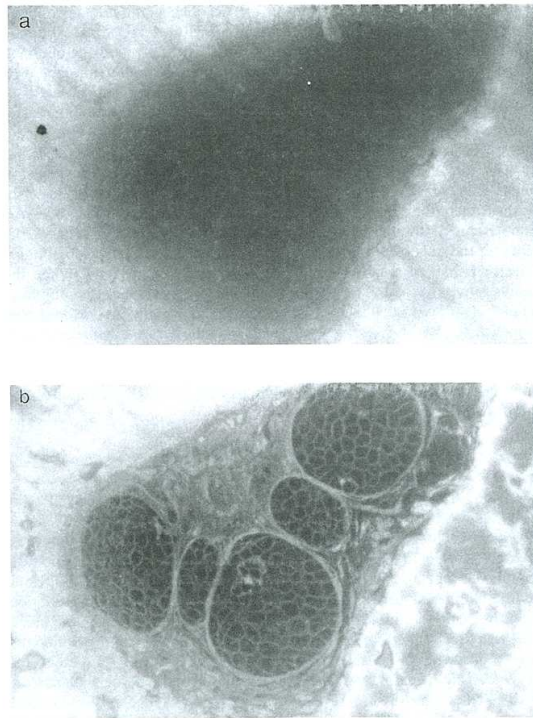


Figure 44: Human bone cell, ordinary (top) and confocal (bottom) microscope image. [from Corle/Kino "Confocal Scanning Optical Microscopy"]

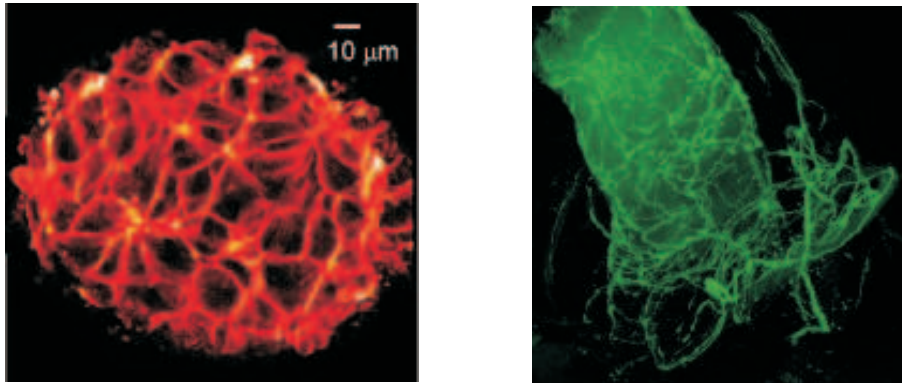


Figure 45: Left: Living pancreatic islet of Langerhans stained with a lipid-soluble fluorescent dye. Right: cGMP-containing cells marked with CY3 running along the antenna nerve of the silkworm. [from Olympus FV1000MPE brochure

Single molecule spectroscopy:

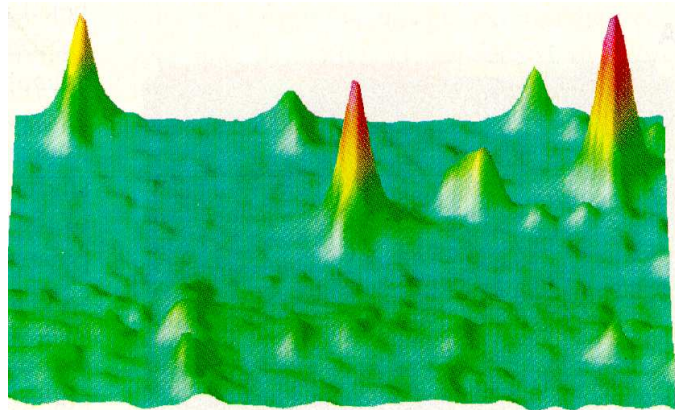


Figure 46: SCOM-image of single GFP molecules (scan rate 10ms per pixel).

We further discuss the detection of single molecule detection in the following subsection.

3.2 Single Molecule spectroscopy

3.2.1 Basics

More than 30 years ago it was shown that it is possible to detect a single molecule in its natural (fluid) environment [T. Hirschfeld, Appl. Opt. 15, 2965 (1976)]. In this experiment the single molecule was stained with a large number of fluorophores.

Follow-up experiments in the early 90s succeeded in optical detection of a single fluorescent molecule (in a solid matrix by Moerner et al., Phys. Rev. Lett., 62, 2535 (1989) and in a liquid stream by Shera et al., Chemical Physics Letters 174, 553 (1990)).

Motivation for single molecule experiments:

- ultimate limit of an optical detection method
- development of highly sensitive imaging with the help of optical markers (labeling)
- investigation of (biological) processes beyond the ensemble average

The difficulty of the detection of a single molecule in natural environment, i.e., in a solid matrix or liquid solution, stems from the tiny signal within a huge background from surrounding molecules (on the order of 10^{23} !).

It is interesting to derive an **estimation of the expected signal** in single molecule microscopy:

The number of photons N_p detected from a single molecule within a certain integration time T_{int} and under a certain excitation intensity P_0 is:

$$N_p = \eta \phi \sigma P_0 T_{int} / (A h \nu) \quad (204)$$

where η is the detection efficiency, ϕ is the quantum efficiency, σ the absorption cross-section and A the effective excitation area. Typical values for these variables are:

$$\begin{aligned} \eta &= 10\% \\ \phi &= 0.5 \\ \sigma &= 1.4 \text{ \AA}^2 \quad (\text{Texas Red}) \\ \sigma/A &= 5 \cdot 10^{-6} \quad (\text{SNOM}) \end{aligned}$$

With an absorption rate of 10^6 photons per second one has approximately 50.000 photons per second.

Possible noise sources disturbing the measurement are:

- shot-Noise (because of the granular nature of photons)
- induced background fluorescence
- dark counts from the detector

Taking these sources into account (assuming a Poissonian process for the shot noise) the following expression can be derived for the signal-to-noise-ratio (SNR):

$$SNR = \frac{\eta\phi\sigma P_0 T_{int}/A h\nu}{\sqrt{\eta\phi\sigma P_0 T_{int}/A h\nu + CP_0\tau + N_{dark}\tau}} \quad (205)$$

If shot-noise is the dominant term, then a SNR of more than 220 is possible.

From the simple estimation it is possible to derive requirements for single molecule detection:

- The detection efficiency (loss in optical system and detector efficiency) has to be as large as possible, e.g., by using a high-NA objective.
- The quantum efficiency and absorption cross-section of the molecules (ideally dye molecules) has to be large.
- The excitation area A should be as small as possible. (The excitation volume also contributes to the constant C !)

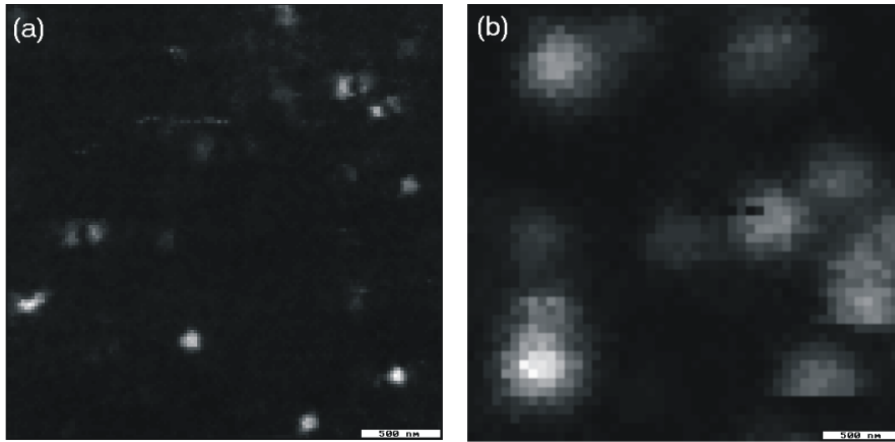


Figure 47: Single Texas Red dye molecules under near- and wide-field illumination (scale bar 500 nm).

The dynamics within a molecule (time evolution of the population of individual energy levels) is typically described by a rate equation model. The following figure 48 shows a Jablonski-diagram of a simple molecule:

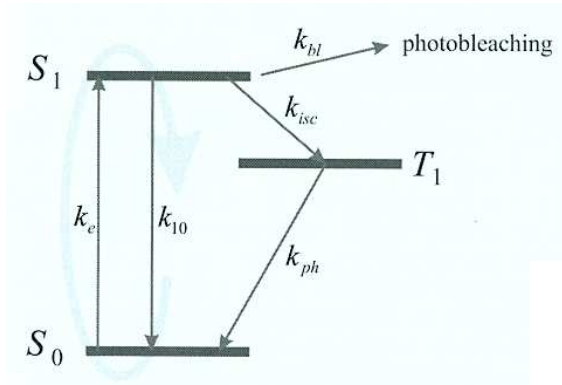


Figure 48: Jablonski-diagram of a simple molecule [from Zander et al. "Single Molecule Detection in Solution"]

One can immediately derive the rate equations from the Jablonski-diagram:

$$\partial_t s_0 = -k_e s_0 + k_{10} s_1 + k_{ph} t_1 \quad (206)$$

$$\partial_t s_1 = k_e s_0 - k_{10} s_1 - k_{isc} s_1 - k_{bl} s_1 \quad (207)$$

$$\partial_t t_1 = k_{isc} s_1 - k_{ph} t_1 \quad (208)$$

The measurable fluorescence rate $k_f(r, t)$ can be derived from the quantum efficiency ϕ_f and the spatial dependent collection efficiency $\eta(r)$:

$$k_f(r, t) = \frac{\eta(r)\phi_f}{\tau} s_1(r, t) \quad \text{with} \quad (209)$$

$$\tau = (k_{10} + k_{isc} + k_{bl})^{-1} \approx k_{01}^{-1} \quad (210)$$

From the equation above the quantum efficiency is defined ϕ_f as:

$$\phi_f = \frac{k_{10}}{k_{10} + k_{isc} + k_{bl}} \quad (211)$$

Typically it is

$$\phi_{bl} = \frac{k_{bl}}{k_{10} + k_{isc} + k_{bl}} \approx \frac{k_{bl}}{k_{10}} = 10^{-5} \dots 10^{-6} \quad (212)$$

This means that one obtains about 10^5 to 10^6 photons from a single molecule before *photo-bleaching* occurs.

The molecular dynamics can be subdivided in different time scales: The fastest is given by the largest rate $(k_{01})^{-1}$, which is about 10^{-9} s. The slowest is determined by $(k_{bl})^{-1}$, which is typically in the regime of milliseconds.

If one assumes - for short times - that

$$s_{tot} = s_0 + s_1 + t_1 \quad (213)$$

is constant, it is straightforward to solve the rate equations, and one derives a simple solution for $s_1(t)$ with a stationary value

$$\bar{s}_1 = \frac{k_e k_{ph} s_{tot}}{k_e k_{isc} + (k_e + k_{10} + k_{isc}) k_{ph}} \quad (214)$$

The following figure 49 shows the time evolution:

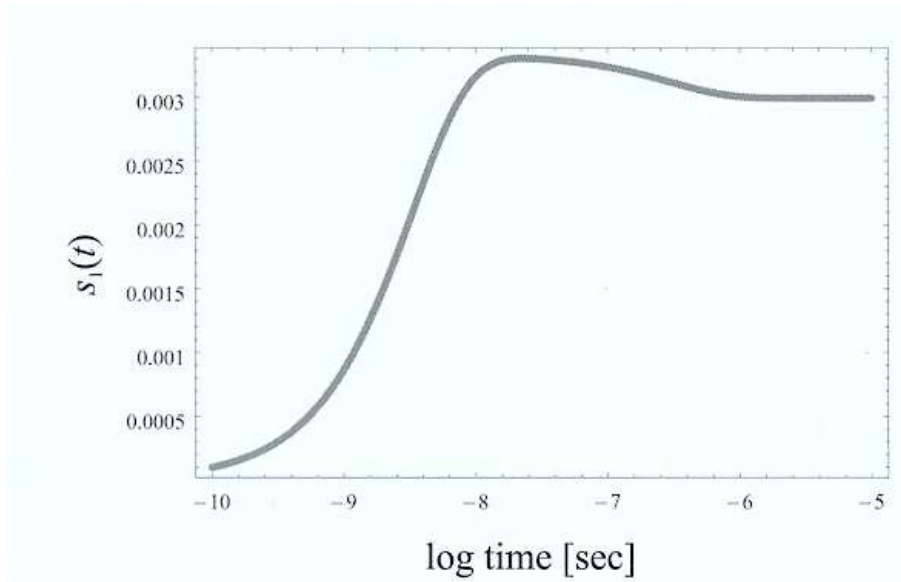


Figure 49: Short-time evolution of the excited state population of a single molecule [from Zander et al. "Single Molecule Detection in Solution"]

For longer times there is a simple exponential decay due to photo-bleaching

$$s_{tot}(t) = s_{tot,0} \exp(-\kappa_{bl}t) \quad (215)$$

In the case of a single molecule there is a rather complicated time evolution (non-Markovian dynamics), as each detection of a photon projects the molecule on a specific state s_{tot} (in the limit of a detection probability of one and no noise $s_0 = 1$).

The following figure 49 shows the time evolution: The following figure 50 shows the behavior

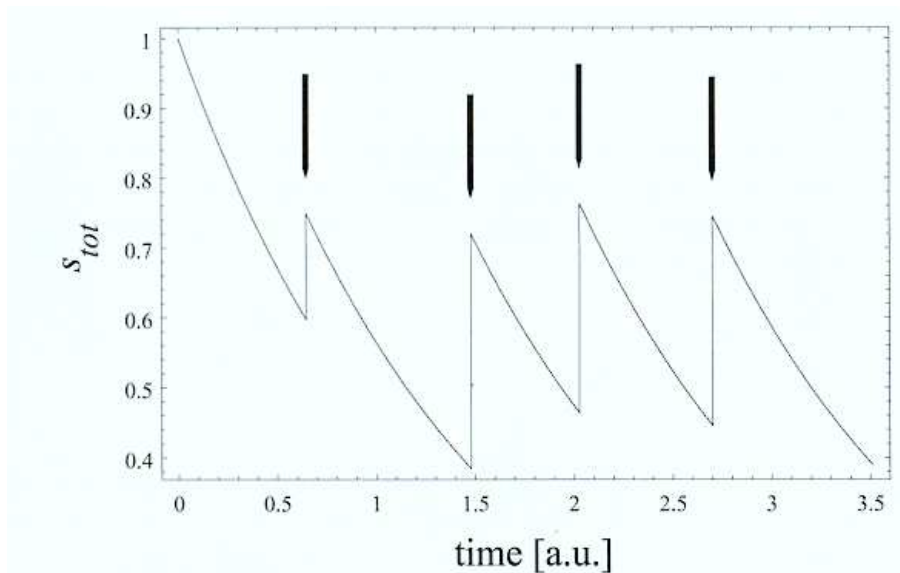


Figure 50: Non-Markovian time evolution of s_{tot} . Arrows mark photon detection events. [from Zander et al., "Single Molecule Detection in Solution"]

In order to characterize a molecule by observation of the emitted intensity a method is required that always resets the molecule in the same initial state.

3.2.2 Methods for data analysis in single molecule spectroscopy

There are different methods to characterize and classify molecules:

1. Burst Size Distribution Analysis

This method is applied if molecules are dissolved in solution and pass a detection zone in a liquid stream. The number of photons from passing molecules, a 'burst' is registered. This number depends on molecular parameters, such as absorption cross-section, lifetime, etc., and allows characterization of the molecules.

The data is then compared to a statistical model. The probability that m molecules pass the detection zone and emit n photons per integration time is calculated.

In case of a highly diluted solution there is in general only one molecule at a time passing the detection zone. A Poissonian distribution of the number of emitted photons can be assumed if the detection probability is low and if the passage time is not too long:

$$p_n = \frac{\bar{n}^n}{n!} \exp(-\bar{n}) \quad (216)$$

2. Fluorescence Intensity Distribution Analysis

This method is similar to the one described above, but the number of photons within a fixed time interval τ is analyzed. The method can thus also be applied to immobilized molecules, e.g., in a solid matrix or a film.

3. Fluorescence Decay Time Analysis

This method determines the lifetime of individual molecules. A pumped laser is used for excitation and all emitted photons are detected as a function of time (Time correlated single photon counting, TCSPC). Obviously, each molecule has a well defined initial state. Figure 51 shows a measured decay curve.

In contrast to the two previously described methods this method is independent of excitation intensity and detection efficiency. The form of the decay curve (mono- or multi-exponential) can be compared to a theoretical rate equation model. TCSPC can also be performed as a function of the excitation or detection wavelength.

4. Autocorrelation Analysis

This method reveals the molecular dynamics, although it is a cw method. The autocorrelation is method as a function of the time delay t between detection events:

$$G^{(2)}(t) = \langle I(0)I(t) \rangle \quad (217)$$

i.e., after the detection of a single photon at time $t_0 = 0$ (reset!) the probability to detect another photon at time $t_0 + t$ is determined.

For n molecules and a background intensity of I_{bg} one finds

$$I(t) = \sum_j^n I_j(t) + I_{bg}(t) \quad (218)$$

and therefore

$$G^{(2)}(t) = \sum_j \langle I_j(0)I_j(t) \rangle + \sum_{j \neq k} \langle I_j \rangle \langle I_k \rangle + 2 \langle I_{bg} \rangle \sum_j \langle I_j \rangle + \langle I_{bg} \rangle^2 \quad (219)$$

$$= n \langle I(t_0)I(t_0 + t) \rangle + n(n-1) \langle I \rangle^2 + 2n \langle I_{bg} \rangle \langle I \rangle + \langle I_{bg} \rangle^2 \quad (220)$$

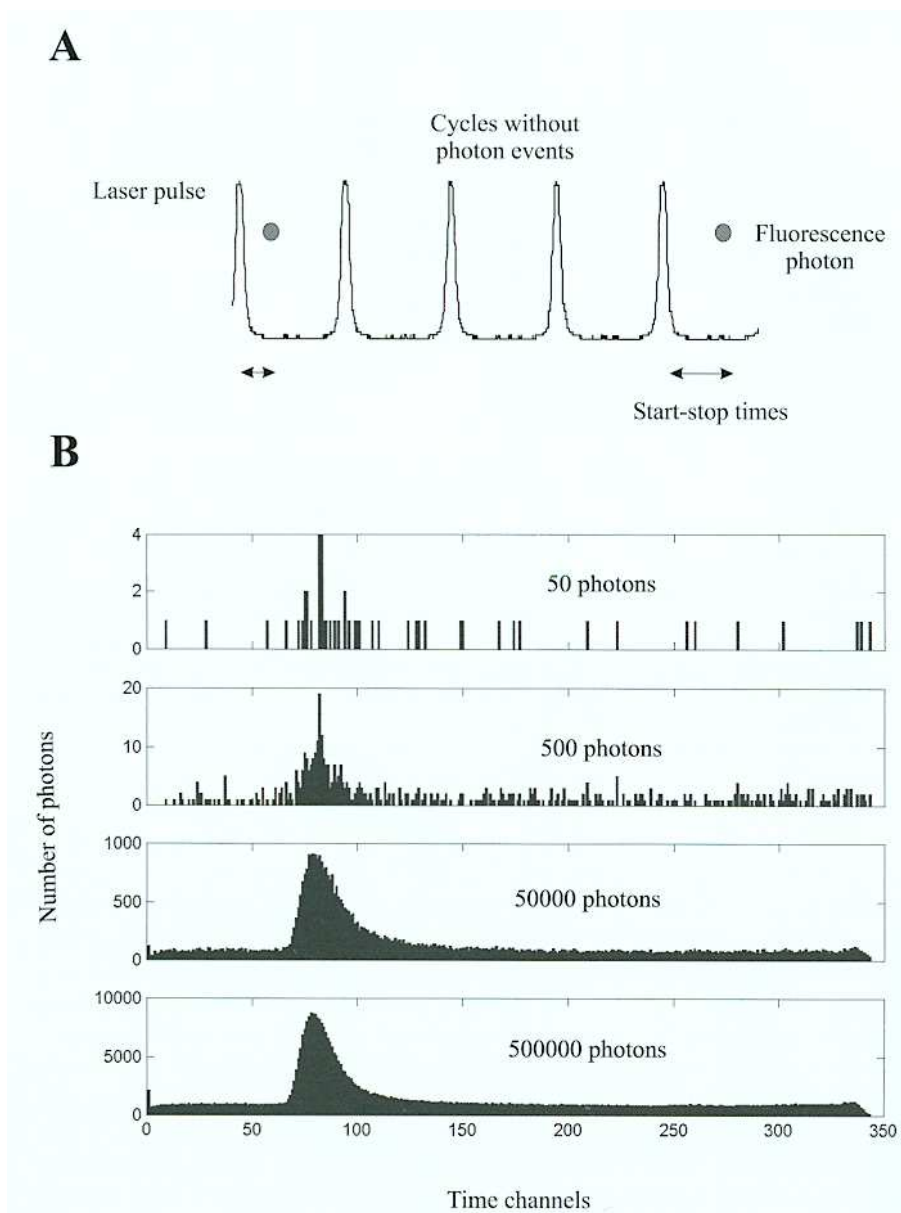


Figure 51: Time correlated single photon counting (TCSPC). A) Schematics and B) measurement result [from Zander et al. "Single Molecule Detection in Solution"]

If diffusion of molecules out of the detection area is taken into account one finds:

$$\langle I(t_0)I(t_0 + t) \rangle = V^{-1} \tau^{-1} \sigma \phi_f^2 \int dr_1 \int dr_0 \frac{\eta(r_1) s_1(r_1, t) \eta(r_0) I_e(r_0)}{[4\pi Dt]^{3/2}} \exp \left[-\frac{|r_1 - r_0|^2}{4Dt} \right]$$

with a diffusion constant D .

For short times t diffusion and photo-bleaching can be neglected and the time dependence is determined by $s_1(t)$ (s. curve above). Therefore, it is possible to derive the rates k_{10} , k_{isc} and k_{ph} ! The following figure 52 shows as an example the singlet/triplet dynamics of the laser dye Rhodamin 6G:

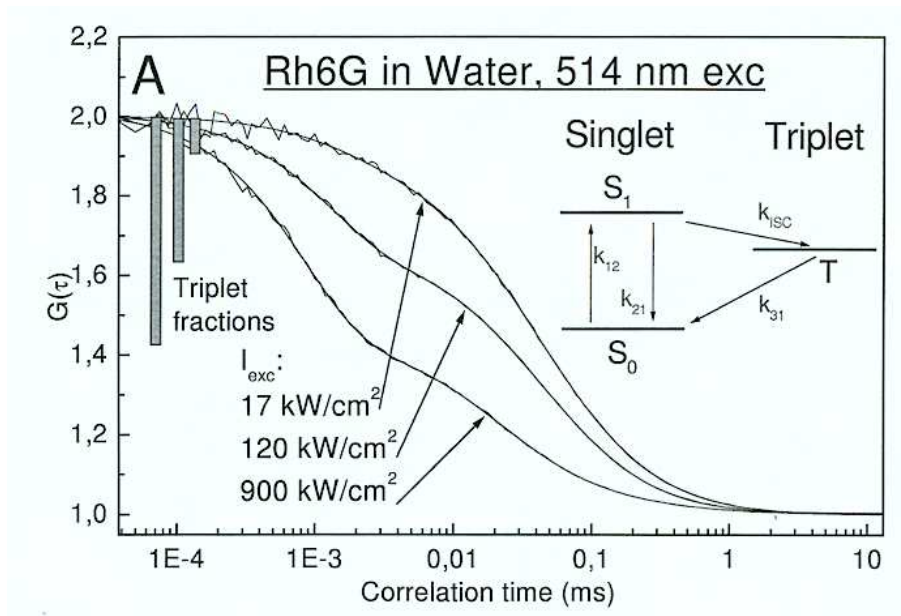


Figure 52: Measured autocorrelation function of Rhodamin 6G for different excitation intensities [from Zander et al. "Single Molecule Detection in Solution"]

For long times the stationary value \bar{s}_1 (equation 214) for $s_1(t)$ can be inserted. In this case one finds for the limit $G^{(2)}(t \rightarrow \infty) \equiv G_\infty$ and $G^{(2)}(t \rightarrow 0) \equiv G_0$ the result:

$$\frac{G_0 - G_\infty}{G_\infty} = \frac{1}{c} \frac{\int dr_0 [\eta(r_0)I_e(r_0)]^2}{[\int dr_0 \eta(r_0)I_e(r_0)]^2} \quad (221)$$

with the molecule concentration $c = n/V$. The expression on the right is thus inversely proportional to the concentration of the molecules, i.e. c is multiplied by a constant factor which does not depend on photophysical parameters of the molecules! Thus, the relative or (with known parameters of the optical systems) the absolute concentration c can be measured.

3.2.3 Optical Tweezers

An **Optical Tweezer** is a focussed laser beam which is used to trap small dielectric particles [Ashkin et al., Opt. Lett. 11, 288 (1986)].

The following figure 53 shows the forces acting on a dielectric sphere in the focus of a laser beam:

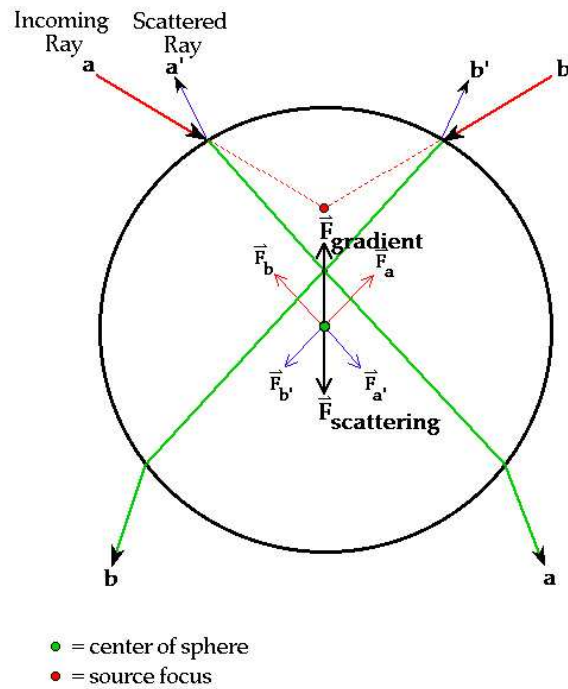


Figure 53: Scattering and gradient force in a dielectric sphere [<http://www.lightforce.harvard.edu/>]

There are two contributions:

1. Scattering force (dashed arrows in figure 53)
This force drives the sphere in the propagation direction of the laser beam (light pressure).
2. Gradient force
This force is due to the momentum change when diffracting light at the air/sphere boundary.

If the gradient force exceeds the scattering force (and if the index of refraction of the sphere is larger than its surrounding medium) then a trapping of the sphere in the laser focus is possible.

Figure 54 shows the directions of the resulting force acting on the sphere for different positions within the laser beam:

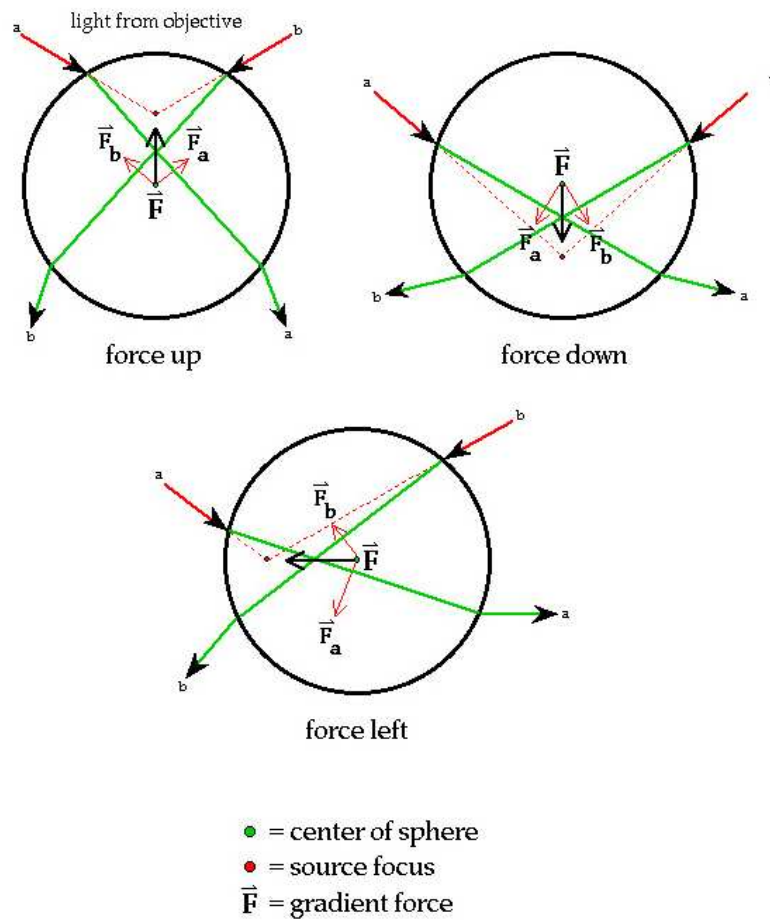


Figure 54: Resulting forces on a dielectric sphere in a focussed laser beam [<http://www.lightforce.harvard.edu/>]

Typically, optical tweezers utilize focussed Gaussian TE₀₀ modes. An exact treatment results in the following forces acting on a dielectric particle with dielectric constant ϵ in a surrounding medium with dielectric constant ϵ_0 :

$$F = F_S + F_{\nabla} \quad (222)$$

$$F_S = \frac{8}{3}\pi(ka)^4 a^2 \frac{\sqrt{\epsilon_0}}{c} \left(\frac{\epsilon - \epsilon_0}{\epsilon + 2\epsilon_0} \right)^2 S \quad (223)$$

$$F_{\nabla} = 2\pi a^3 \frac{\sqrt{\epsilon_0}}{c} \left(\frac{\epsilon - \epsilon_0}{\epsilon + 2\epsilon_0} \right) \nabla |S| \quad (224)$$

Here S is the Poynting vector.

In case of $\epsilon > \epsilon_0$ the gradient force is along the intensity gradient of the focussed light in the direction of increasing intensity (towards the focus).

A more general ansatz starts with the dipole potential:

$$V_{dipol} = -d \cdot E \quad (225)$$

In a linear medium it is

$$V_{dipol} \propto -\alpha E \cdot E \quad \text{und} \quad (226)$$

$$F_{dipol} = -\nabla V_{dipol} \propto \alpha \nabla (|E|^2) \quad (227)$$

This **dipole force** acts in the direction of the intensity gradient. Its sign depends via the polarizability α on the frequency of the laser field. Below a characteristic resonance the dipole force attracts the dielectric particle towards the focus (into the highest intensity), above the resonance the particle is expelled (attracted towards lowest intensity).

Figure 55 shows a simple experimental setup for an optical tweezers.

The setup resembles a beam-scan confocal optical microscope. Tilting of the beam is realized via moving one of the telescope mirrors. Imaging of the trapped particle on a quadrant detector determines the exact position of the particle with few nm resolution.

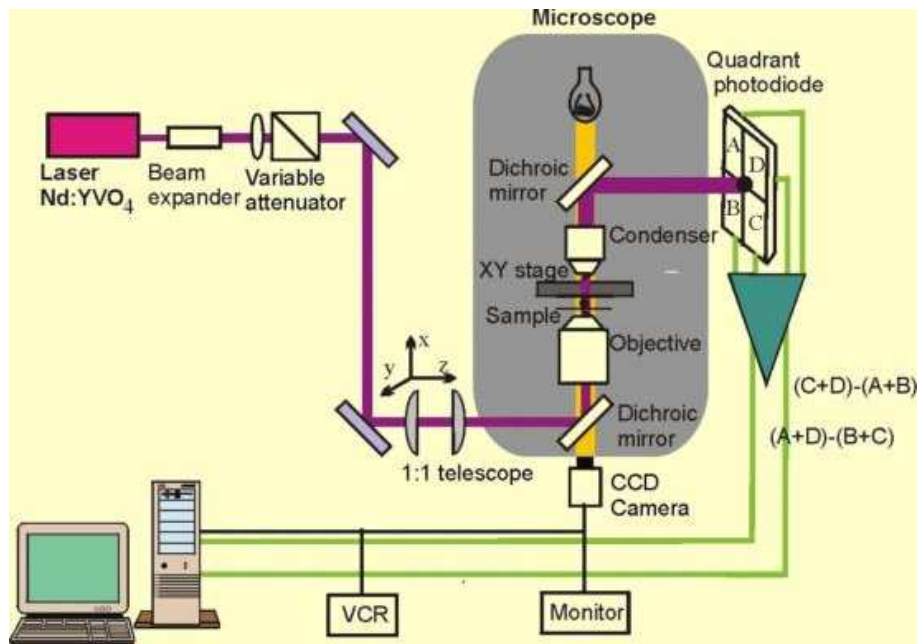


Figure 55: Simple setup for optical tweezers.

The following figure 56 provides some typical values for trapping a polystyrene sphere:

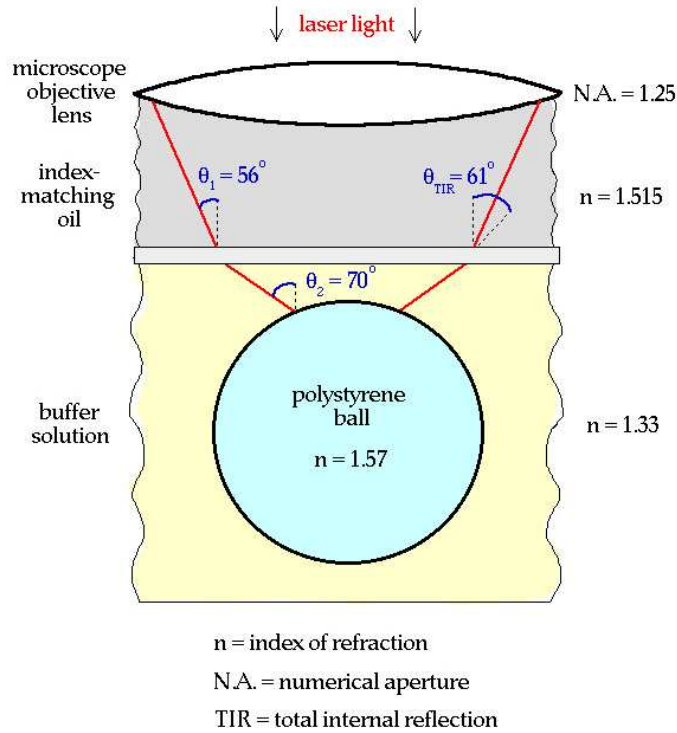


Figure 56: Schematics and typical values for trapping a polystyrene sphere.

With multiple beams it is possible to trap and manipulate a larger number of particles. There are two ways to realize multiple-beam optical tweezers:

- A laser beam is rapidly switched between two different positions. Because of the inertia of the trapped particles in the viscous medium this results in two separated effective trapping potentials.
- The laser beam is diffracted through a diffractive element. An arbitrary pattern of different laser spots (trapping potentials) can be generated in this way.

The following figure 57 shows an experimental setup and several trapped particles.

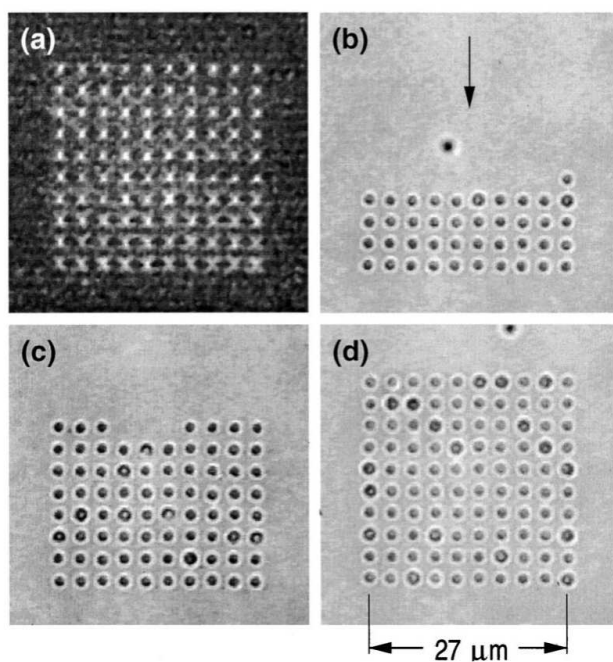
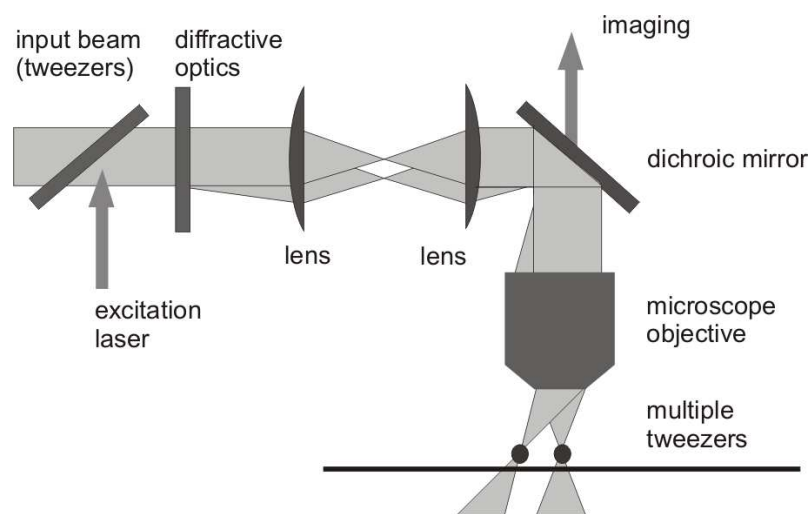


Figure 57: Schematics of multi-beam tweezers. 10x10 array of multiple optical tweezers. (a) Tweezers focussed on a glass substrate, (b)...(d) trapping of glass spheres [from Korda et al., Rev. Sci. Instr. 73, 1956 (2002)]

An important parameter of optical tweezers (or optical trap) is the trap depth. A calibration of the trapping potential is possible via Brownian motion, assuming a harmonic trapping potential.

The average force acting on the particle is:

$$F(\langle x \rangle, t) = \kappa \langle x \rangle + \gamma \dot{\langle x \rangle} \quad (228)$$

with the spring constant (of the trap) κ and the damping constant (of the viscous medium) $\gamma = 3\pi\eta d$. Here d is the particle diameter and η is the viscosity constant. Inertia of the particles can be neglected for small particles in a liquid.

After Fourier transformation of the fluctuations $x(t)$ one derives the spectrum:

$$S(f) = \frac{k_B T}{\gamma \pi^2 (f^2 + f_c^2)} \quad (229)$$

$$f_c = \kappa / 2\pi\gamma \quad (230)$$

Thus, measuring the critical frequency in the spectrum of the fluctuations $x(t)$ reveals the spring constant κ of the trap. It is typically on the order of

$$\kappa \approx 1 \text{ pN/nm} \quad (231)$$

and depends on the laser intensity (some 100 mW).

With the help of the spring constant it is possible to calibrate the fluctuations:

$$\langle x^2 \rangle = \frac{k_B T}{\kappa} \quad (232)$$

Thus observation of exact particle position with respect to the trap center allows measuring very small forces.

Brownian motion sets a limit to the minimum size of particles which still can be trapped. Too small particles can escape from the trap. Obviously, the trapping potential can not be increased arbitrarily by increasing the laser power (heat!). However, trapping of particles well below 100 nm is possible in solution at room temperature.

3.2.4 Detection and manipulation of small bio-molecules

Optical tweezers are an ideal tool to investigate bio-molecules because of the following reasons:

- non-invasive manipulation technique with nm precision
- ease of integration and combination with ordinary (confocal) microscopes
- precise measurement of particle positions (nm-regime)
- measurement of small forces (pN-regime)

A typical approach is to coat dielectric particles with specific functional groups. These attach to corresponding bio-molecules.

In the following we provide 4 examples for applications of optical tweezers in biophysics:

1) Harada et al., Single Molecule Imaging of RNA Polymerase-DNA Interactions in Real Time, *Biophys. Journal* 26, 709 (1999)

In this experiment an optical tweezers is used to hold a DNA-strand. A polymerase molecule labeled with fluorescent markers is observed while moving along the DNA-strand. Illumination of markers is done in an evanescent field.

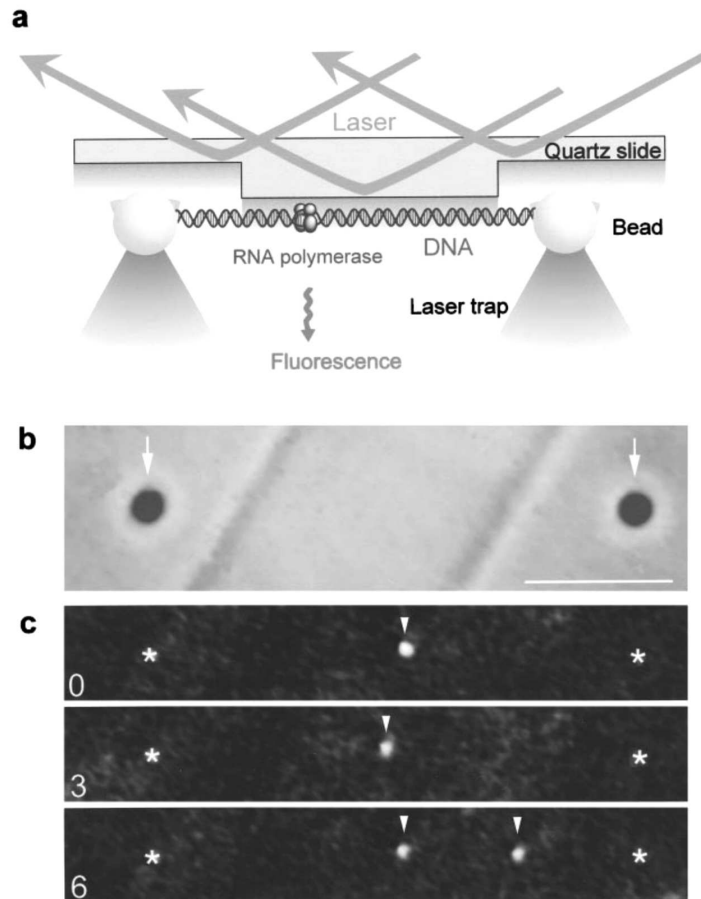


Figure 58: A RNA-polymerase molecule moving along a trapped DNA-strand: a) schematics, b) microscope image of two trapped 'beads', c) fluorescence image of the RNA-polymerase

2) Baumann et al., Stretching of Single Collapsed DNA Molecules, Biophys. Journal 78, 1965 (2000)

In this experiment a tweezers is used to stretch a DNA fragment. All large proteins are folded or wind-up chains. The forces when unwinding a protein reveals information of its conformation.

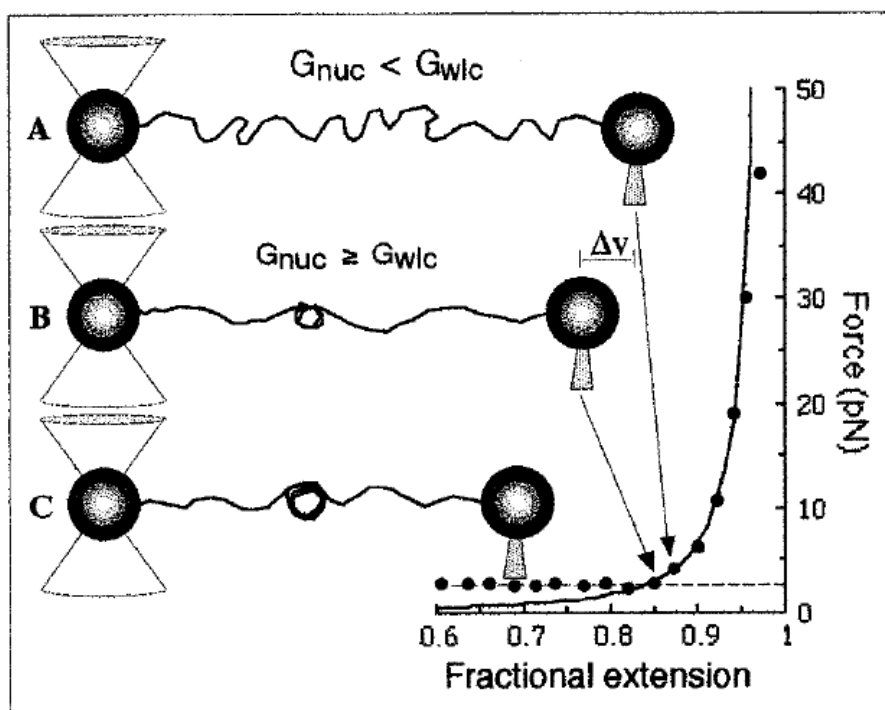


Figure 59: Stretching of a DNA fragment with the help of optical tweezers. Points are measured forces, the solid line is a theoretical model.

3) Bockelmann et al., Unzipping DNA with Optical Tweezers: High Sequence Sensitivity and Force Flips, *Biophys. Journal* 82, 1537 (2002)

One strand of a DNA double-helix is mounted on a cover slip the other is attached to a 'bead'. The position of the bead is used to measure the force when unzipping the DNA helix. Breaking of the binding of base pairs can be observed.

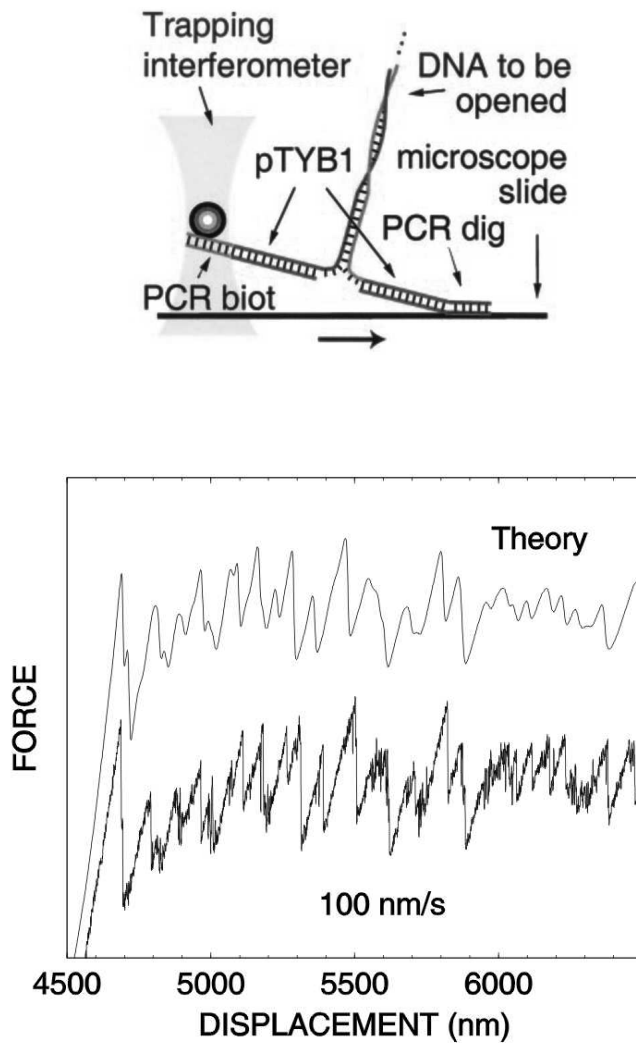


Figure 60: Top: Schematics of the experiment; Bottom: Measured force when unzipping the DNA double-helix.

4) Lang et al., An Automated Two-Dimensional Force Clamp For Single Molecule Studies, *Biophys. Journal* 83, 491 (2002)

The experiment investigates so-called 'motor molecules'. These molecules perform a mechanic motion, e.g. a rotation or translation along a filament.

- The motion occurs in discrete steps. Such steps cannot be revealed in an ensemble measurement!
- The mechanic motion consumes energy in discrete units (number of consumed ATP-molecules)
- Motion of small objects in a viscous medium is dominated by friction, and thus very different from macroscopic motion. For example, motion under an applied force occurs only *on the average* in a specific direction. The statistic nature of individual steps of the motion can only be observed in a single molecule measurement.

Widely studied motor molecules are Myosin and Kinesin, which move along actin filaments (filaments within the cytoplams of cells).

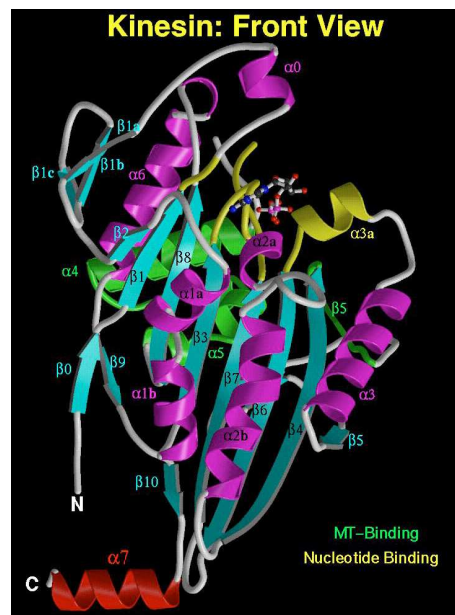


Figure 61: Structure of the Kinesin molecule.

The following figure shows an experimental setup to study the motion of 'motor molecules':

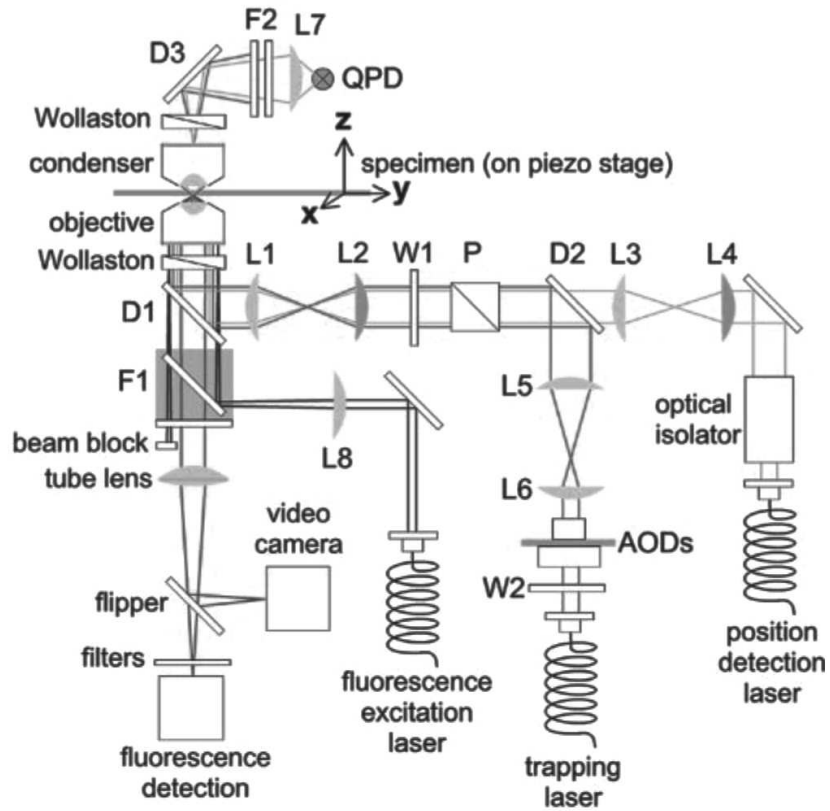


Figure 62: Schematics of the experimental setup. There are three laser beams for the optical tweezers, position detection and fluorescence excitation.

The experiment is performed as follows:

- A) Trapping of a bead.
- B) Trigger, Kinesin pulls the bead towards the detection volume.
- C) Alignment of the bead with respect to the calibrated detector zone.
- D) Movement of the tweezers to maintain a constant force.

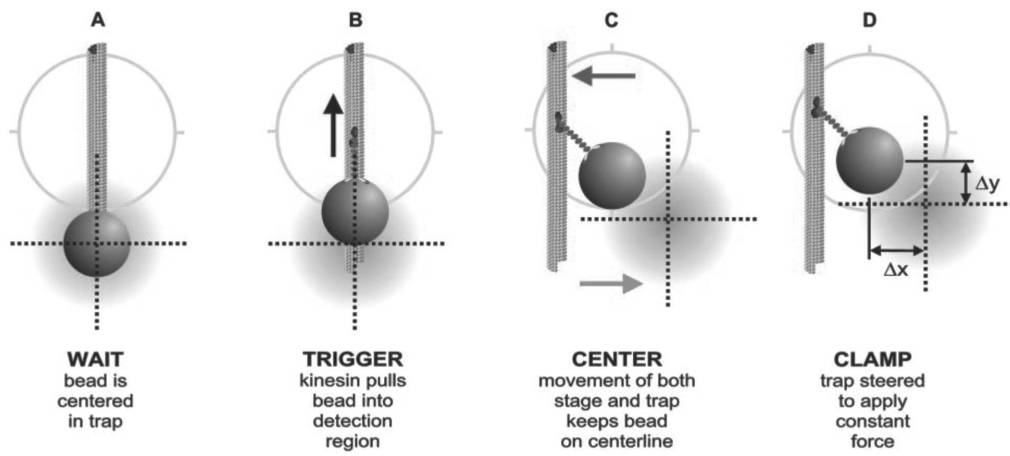


Figure 63: Schematics of the experiment (see text).

The following figure shows a measurement result.

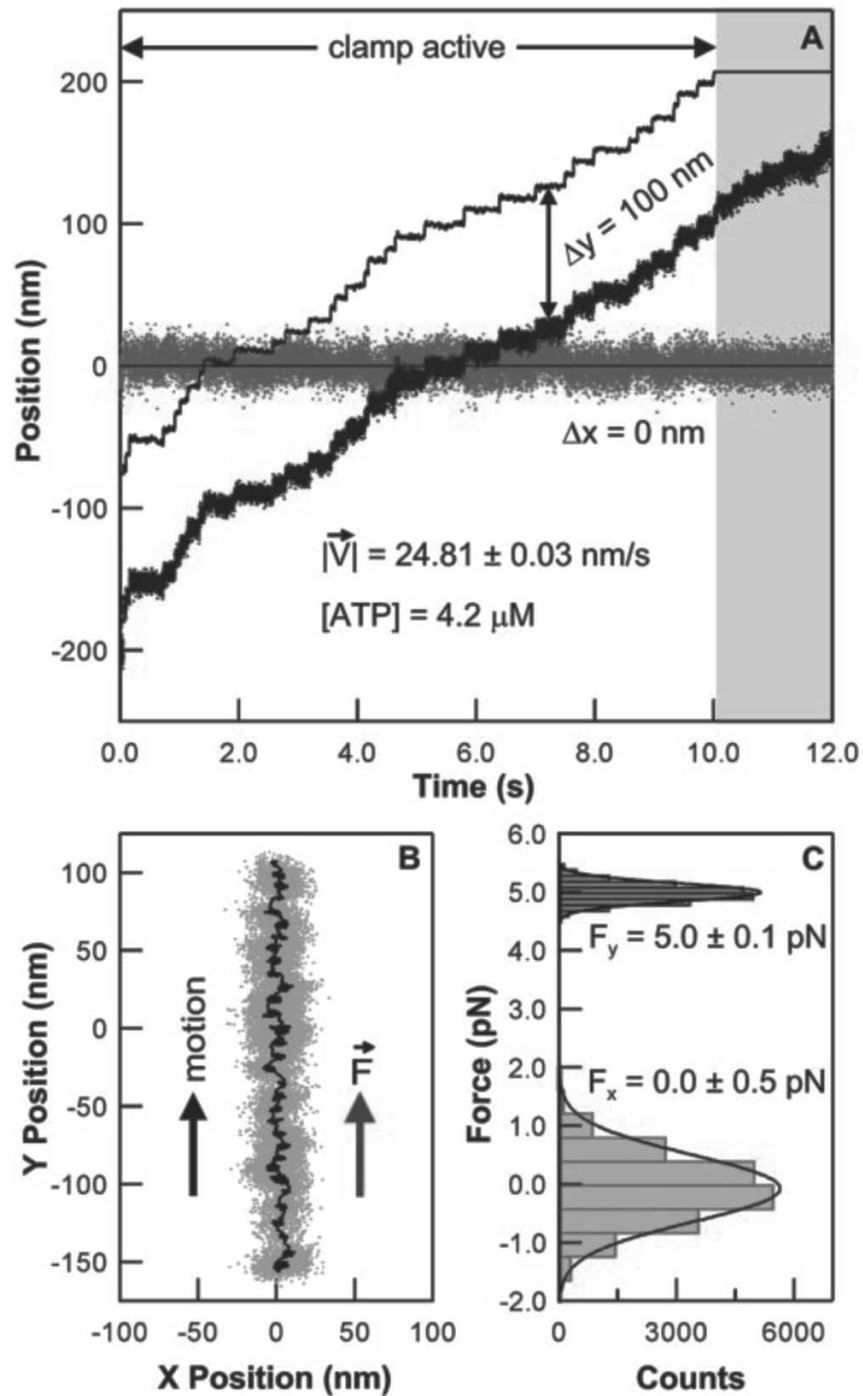


Figure 64: a) Motion of the Kinesin molecule along y-direction (upper diagonal curve) and x-direction (middle straight curve). The upper curve is the signal of the position detector, while the lower curve is the signal of the tweezers. b) x- and y-motion, c) Histogram of the average force in x- and in y- direction

3.3 STED microscopy

3.3.1 General principle

When deriving the PSF for confocal microscopy we pointed out that a non-linear interaction (e.g., two-photon absorption) may further increase the resolution in the far-field.

One reason for a non-linear behavior is *saturation*. S. Hell suggested in 1994 to use saturation in fluorescence imaging and later demonstrated a breaking of the Abbe limit (Klar, T. A. and Hell, S. W. (1999) *Opt. Lett.* 24, 954956.). *Stimulated Emission Depletion (STED)* microscopy combines excitation and stimulated emission of a fluorescence dye by two appropriately shaped laser pulses in order to enhance the resolution.

Assume the following typical level scheme for a fluorescent dye:

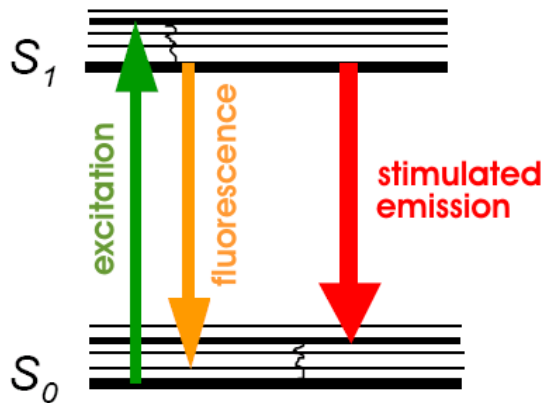


Figure 65: Schematic level diagram of a dye molecule [from homepage S. Hell, Göttingen].

There are two ingredients for STED:

1. pulsed laser with an intensity profile with a zero at the origin (e.g. a doughnut shape)
2. target material with reversible saturable linear transition

Now STED works as follows:

1. Excitation is performed by a subpicosecond laser pulse that is tuned to the absorption spectrum of the dye. The excitation pulse is focused into the sample, producing an ordinary diffraction limited spot of excited molecules.
2. The excitation pulse is immediately followed by a depletion pulse (STED-pulse). The STED pulse is red-shifted in frequency to the emission spectrum of the dye, so that its lower energy photons act ideally only on the excited dye molecules, quenching them to the ground state by stimulated emission. The net effect of the STED pulse is that the affected excited molecules cannot fluoresce because their energy is dumped and lost in the STED pulse. By spatially arranging the STED pulse in a doughnut mode, only the molecules at the periphery of the spot are ideally quenched.
3. Fluorescence is observed only in the center of the doughnut, where the STED pulse is vanishing.

The situation is illustrated in figure 66.

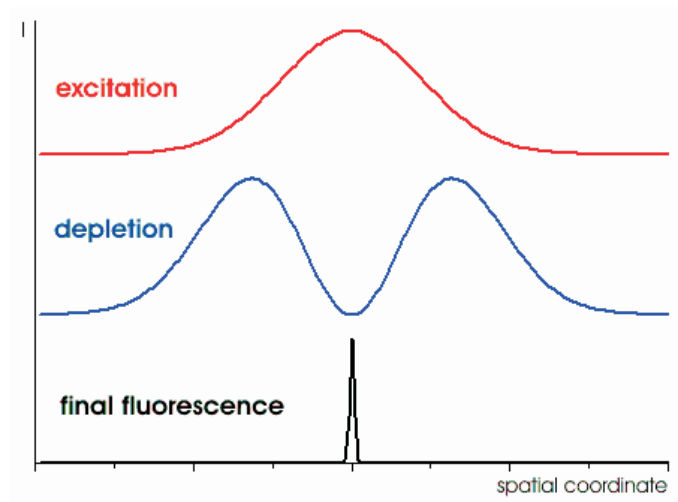


Figure 66: Combination of excitation and depletion pulses in STED microscopy.

The following figures show the measured depletion of fluorescence as a function of the intensity of the STED pulse.

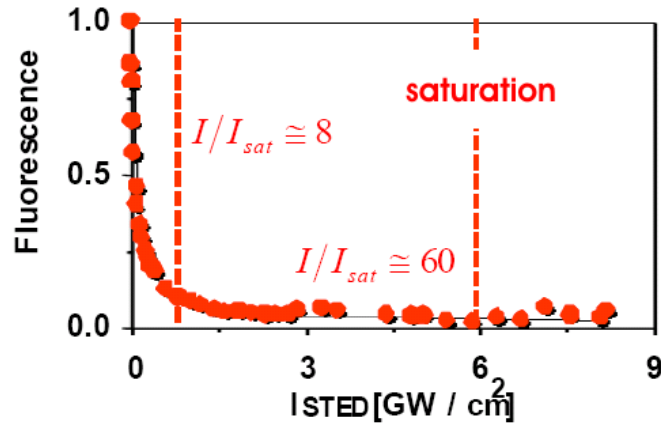


Figure 67: Depletion of fluorescence as a function of STEP-pulse intensity. The quenching is approximately exponential. [from homepage S. Hell, Göttingen].

By increasing the STED pulse intensity, the depletion becomes complete at the spot's periphery and increasingly more effective towards the middle. At the doughnut hole, however, the fluorescence is ideally not affected at all. Therefore, by increasing the intensity of the doughnut-shaped STED-pulse, the fluorescent spot can be progressively narrowed down, in theory, even to the size of a molecule. This concept signifies a fundamental breaking of the diffraction barrier.

The essential idea of STED is the saturated reduction of the fluorescence (=depletion) at any coordinate but the focal point.

The physical reason for the breaking of the diffraction barrier is not the fact that fluorescence is inhibited, but the saturation. Fluorescence reduction alone would not help since the focused STED-pulse is also diffraction-limited.

3.3.2 Resolution in STED microscopy

It is possible to estimate the resolution in STED-microscopy.

Let us assume the following excitation rate for the excited state of the molecule:

$$\gamma_e(r) = \sigma I_e(r)/\hbar\omega_0 \quad (233)$$

where σ is the one-photon absorption cross-section and I_e is the intensity associated with the excitation field.

Once the system is in the excited state the probability of a spontaneous transition to the ground state (fluorescence) is:

$$\frac{\gamma_r}{\gamma_r + \gamma_d} \quad (234)$$

where γ_r is the radiative decay rate and γ_d is the stimulated transition rate. The latter can be written as:

$$\gamma_d(r) = \sigma I_d(r)/\hbar\omega_0 \quad (235)$$

with $I_d(r)$ being the intensity of the depletion field.

Combining the two equations results in an expression for the fluorescence rate γ_f :

$$\gamma_f(r) = \gamma_e(r) \frac{\gamma_r}{\gamma_r + \gamma_d(r)} = \frac{\sigma}{\hbar\omega_0} \frac{I_e(r)}{1 + d_p(r)} \quad (236)$$

where the *depletion parameter* $d_p(r)$ is introduced.

$$d_p(r) = \frac{\sigma}{\hbar\omega_0 \gamma_r} I_d(r) \quad (237)$$

The latter corresponds to the ratio of stimulated and spontaneous emission rates. For a weak depletion $d_p \approx 0$ the fluorescence rate reduces to the ordinary fluorescence rate.

As the depletion parameter can be arbitrarily large (by increasing the intensity of the depletion pulse) only an arbitrarily small spot around the zero of the depletion pulse contributes to the fluorescence.

It is possible to provide an approximate formula for the transversal resolution as follows:

$$\Delta r_{\parallel} \approx 0.6098 \frac{\lambda}{NA \sqrt{1 + d_p}} \quad (238)$$

Any $d_p > 0$ enhances the resolution!

3.3.3 Implementation

It is not too difficult to implement STED in ordinary fluorescence microscope. Figure 68 shows a typical setup:

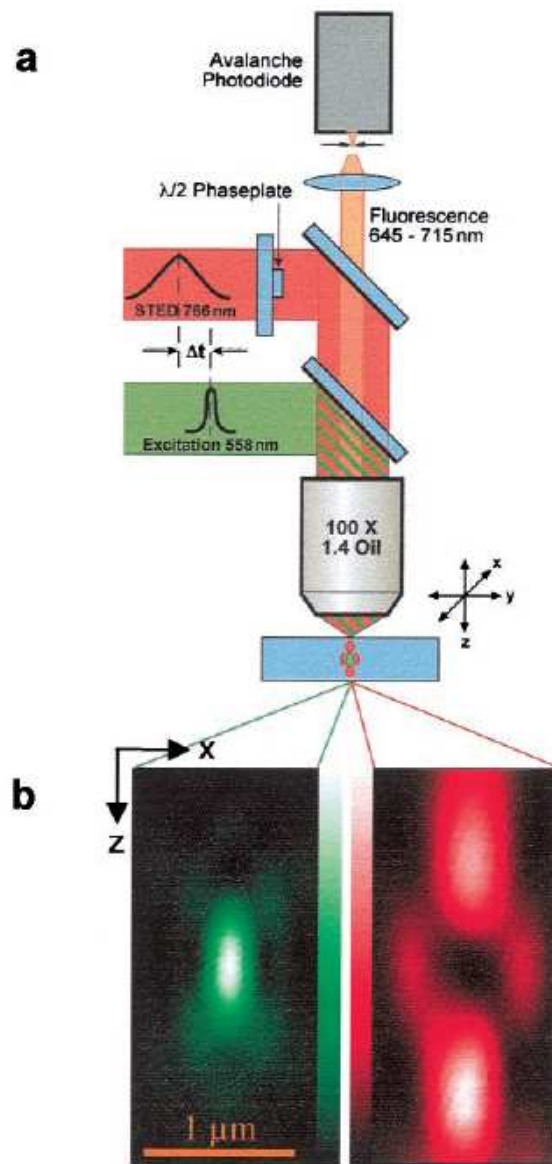


Figure 68: Typical setup of a STED microscope. Note the beam shaping of the STED beam via a phase plate [from Klar et al. PNAS 97, 8209 (2000)].

The following figure 69 illustrates the measured reduction of the fluorescence spot in STED microscopy.

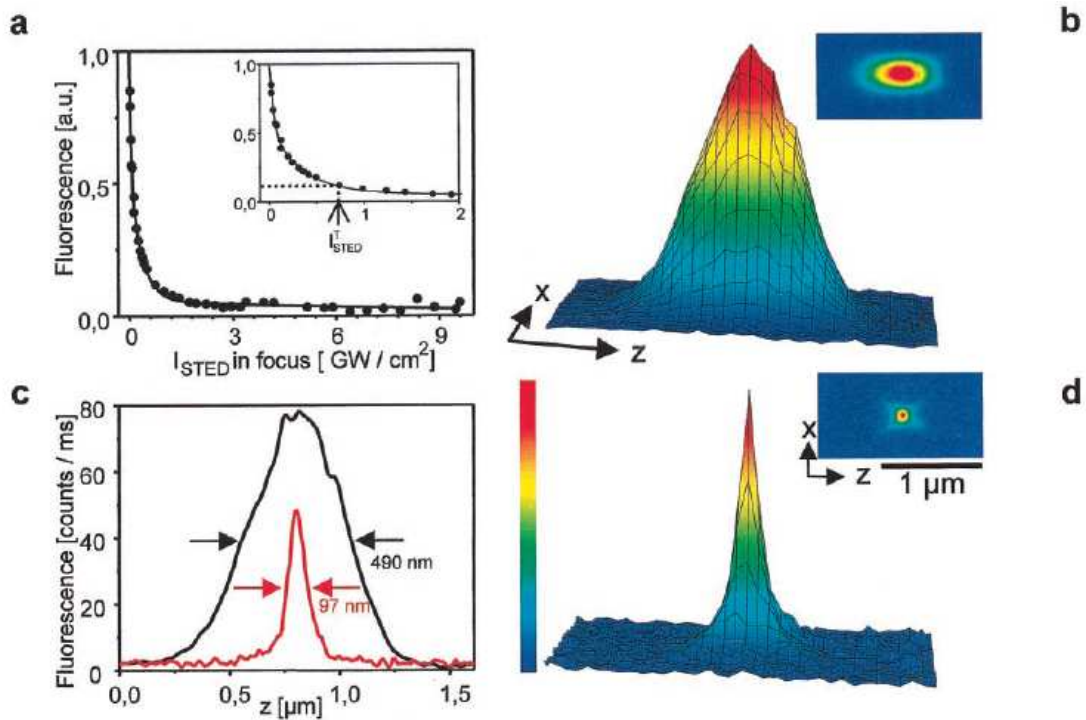


Figure 69: (a) Fluorescence is a nonlinear function of stimulating intensity; 10% remaining fluorescence is obtained for a STED intensity I_{STED} corresponding to a power of P_{STED} of 2.2 mW in the focus. (b) Surface plot of xz -section (Inset) of confocal fluorescence spot for 1.4 oil immersion lens. (d) Same as b but with STED-beam PSF switched on. (c) Corresponding axial intensity profiles demonstrate 5.1-fold reduction of the axial width (FWHM) from 490 nm down to 97 nm. [from Klar et al. PNAS 97, 8209 (2000)].

3.3.4 STED results

STED microscopes are commercially available. The following figures give an impression of the enhanced optical resolution. A limit is presently set by the STED power. Too large intensities photo-bleach the fluorescence dye or deposit too much heat in the sample. The latter is crucial for biological samples.

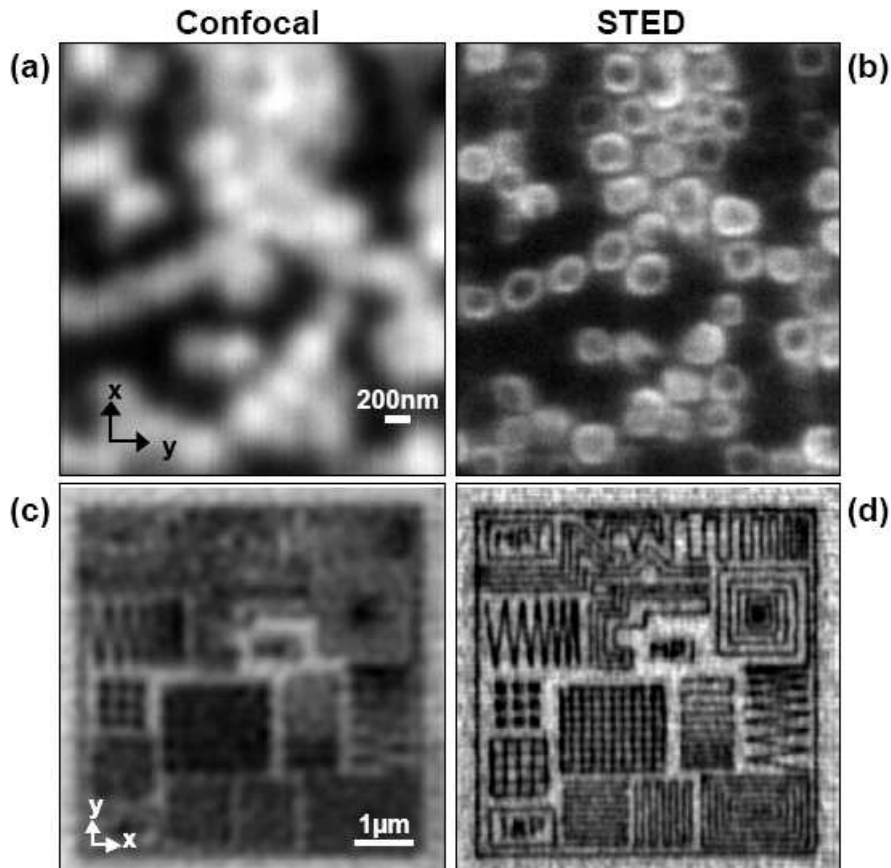


Figure 70: Upper row: Pores in a stained membrane imaged with confocal microscopy (a) and STED microscopy (b); Bottom row: Nanostructures fabricated by e-beam lithography in stained PMMA. Lines are as small as 80 nm with 40 nm separations. Obviously, in both samples a much better resolution is obtained with STED. [from homepage S. Hell, Göttingen]

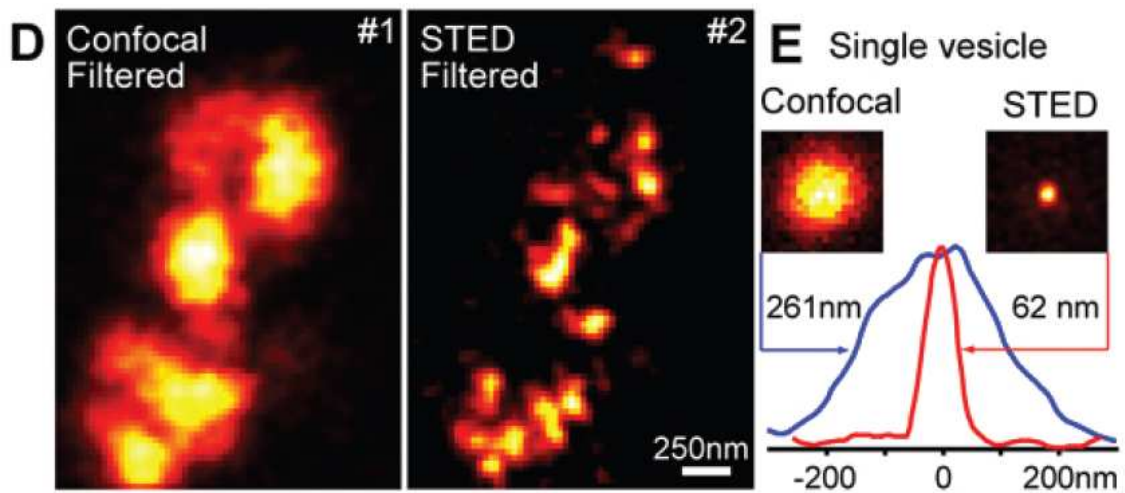


Figure 71: Real-time STED microscopy resolves single synaptic vesicles in living neurons (cultured hippocampal neurons whose surface vesicle pool was labeled with mouse anti-synaptotagmin antibodies and Atto647N-labeled anti-mouse Fab fragments). (D) Smoothing in confocal mode does not improve the differentiation of single objects, while this filtering method helps to identify superresolved vesicles in the STED images. (E) Images of a single stationary vesicle in confocal and STED mode (summed over 10 and 50 frames, respectively) reveal the cross-section of the focal spot in each mode. The line profiles through their center demonstrate the 18-fold reduction in focal spot area. [from Westphal et al., Scienceexpress, 21 February 2008]